frontiers in Materials

REVIEW
published: 01 April 2021
doi: 10.3389/fmats.2021.633079

# Recent Progress of 2D Nanomaterials for Application on Microwave Absorption: A Comprehensive Study

*Muhammed Kallumottakkal*[1], *Mousa I. Hussein*[1]* *and Muhammad Z. Iqbal*[2]

[1]Department of Electrical Engineering, United Arab Emirates University (UAEU), Al Ain, UAE, [2]Department of Chemical and Petroleum Engineering, United Arab Emirates University (UAEU), Al Ain, UAE

Rapid advancements and wide spread of microwave- and RF-communication systems over the years have led to an abundant increase in electromagnetic energy radiation in our living environment. Such an increase in microwave sources is due to the development and advancement in communication techniques (mobile phones, laptops, and antennas for aeronautics or automobile) and electronic warfare in the military field (radar and satellite). Recently research efforts are focused on finding solutions to guarantee protection from electromagnetic (EM) radiations. The EM absorbing materials are used to overcome these issues to ensure public protection as well as safe military operations. Various types of EM absorbing materials comprising composite materials have been progressively developed and researched. This kind of material is developed by impeding absorbing charges (magnetic or dielectric) into a host matrix material. Recently, carbon allotropes such as graphene, MXenes, carbon nanotubes (CNTs), and carbon fibers have attracted increasing attention owing to their EMI shielding characteristics and lightweight. This work presents a comprehensive study on the recent research progress on the application of nanomaterials for electromagnetic shielding and absorption. The review will cover the microwave absorption mechanism and absorption performance using graphene, MXenes, carbon nanotubes (CNTs), carbides, and ferromagnetic metals. Overall, the review will present a timely update on the research progress of microwave absorption performance of various nanomaterials.

**Keywords: 2D nanomaterials, microwave absorption, graphene, MXene, reflection loss**

OPEN ACCESS

***Edited by:***
*Federico Cesano, University of Turin, Italy*

***Reviewed by:***
*Alexander Balandin, University of California, Riverside, United States*
*Xiaobo Chen, University of Missouri–Kansas City, United States*

***Correspondence:**
*Mousa I. Hussein*
*mihussein@uaeu.ac.ae*

***Specialty section:***
*This article was submitted to Carbon-Based Materials, a section of the journal Frontiers in Materials*

***Received:*** *24 November 2020*
***Accepted:*** *25 January 2021*
***Published:*** *01 April 2021*

***Citation:***
*Kallumottakkal M, Hussein MI and Iqbal MZ (2021) Recent Progress of 2D Nanomaterials for Application on Microwave Absorption: A Comprehensive Study. Front. Mater. 8:633079. doi: 10.3389/fmats.2021.633079*

## INTRODUCTION

Because of the increase in environmental emissions of microwave irradiation, microwave absorbing materials (MAMs) have become an essential part of the stealth defensive system for all military platforms (Zhang and Zhu 2009) and communication and information processing technologies (Green and Chen 2019a). The fourth increasing cause of pollution is the microwave radiation, which is considered an extensive threat to the biological system by increasing the chance for cancer, breakdown of DNA strands, and weakening of the immune system (Wang et al., 2013). The research on MAMs started before World War II; in response to the Allies' success with radar sets, Germans had a ferrite-based paint considered as the first radar absorbing material. We have now arrived at advanced nanoabsorbers from conventional absorbers (Delfini et al., 2018). The nanomaterials are effective in enhancing physical, chemical, and electrical properties of base polymers, making them ideal for applications in the fields of energy storage, catalysis, and electronics (Kalambate et al., 2019).

**Figure 1** shows the keyword occurrences in the 2001–2020 SCOPUS documents, showing an exponential increase in interest in this topic over the last two decades.

MAMs are usually coated on the surface of objects to shield them from detection (in the case of stealth fighters) or provide interference (in the case of telecommunication devices) (Liu J. et al., 2020). Heterogeneous nanocomposites comprise an insulating dielectric matrix (rubber, paraffin, or epoxy resin) with a fixed mass ratio (or volume fraction) for microwave absorption studies followed by coating on the metallic surface of the planes (Han et al., 2011). In the same context, operating frequency variance forces researchers to search for materials covering a wide range of absorbing frequencies, where the frequency range depends on the length of the beam bunch and the frequency of the fundamental mode of the accelerating cavity. In current and potential accelerator-based x-ray sources (Chojnacki et al., 2011), bunch length is considered as 1 mm. On the basis of electromagnetic wave components, namely, electrical and magnetic components, microwave absorbers are generally classified into two groups as dielectric or magnetic absorbing materials. Dielectric absorbers rely on electronic polarization, ion polarization, and intrinsic electrical dipolar polarization in their materials to determine the absorption of microwaves. The magnetic absorbers, depending on their magnetic properties (Wang et al., 2013), show a disadvantage of higher density than the dielectric absorbers but exhibit an excellent absorptivity (Munir 2017). These two components should be suppressed simultaneously for better absorption (Silva et al., 2018). MAMs are typically manufactured in sheet form, consisting of insulating/conducting polymers such as rubber, magnetic, or dielectric materials (Munir 2017).

The dimensional classification divides the nanomaterials into 0D, 1D, 2D, 3D structures, and each dimension of the same compound exhibits distinct properties (Rafiei-Sarmazdeh et al., 2019). Two-dimensional nanomaterials are the thinnest nanomaterials among these dimensional groups and have a broad variety of physical, chemical, and electrical properties. Among scientists, 2D material studies are a hot research subject for recent years. This paper provides a comprehensive review of the recent development in the application of 2D nanomaterials for electromagnetic wave absorption such as graphene and MXenes. This manuscript is organized into different sections, starting with the microwave absorption mechanism followed by sections dealing with historical review of carbon nanotubes (CNT) and 2D nanomaterials that are used for microwave applications such as graphene and MXenes.

## MICROWAVE ABSORPTION MECHANISM

The propagating wave hitting MAMs as an obstacle is partially reflected at air-material interface, whereas the other part penetrates through the barrier film and remains absorbed or dissipated as thermal energy inside the material. There is also evidence of secondary reflections and retransmission (Huang et al., 2019) of the absorbed radiation as shown in **Figure 2**. The interaction, absorption, and reflection of these waves are always determined by the magnetic and electric properties of the respective medium and materials through which waves propagate (Tan et al., 2020).

A metal surface is positioned near substrate for reflecting entire waves into the substrate in order to increase absorption capacity. Thus, in microwave absorption with metal background, transmitting waves are negligible, thereby estimating the reflection loss as the difference between the initial incident wave and final reflected wave (Wang et al., 2017). Reflection loss is considered as the main criterion for measuring absorption property. Two conditions must be met by an ideal absorber material: 1) impedance matching between free space and material surface and 2) absorber using dielectric or magnetic losses to attenuate complete EM wave (Silva et al., 2018). A good matching condition of EM impedance can enable almost zero

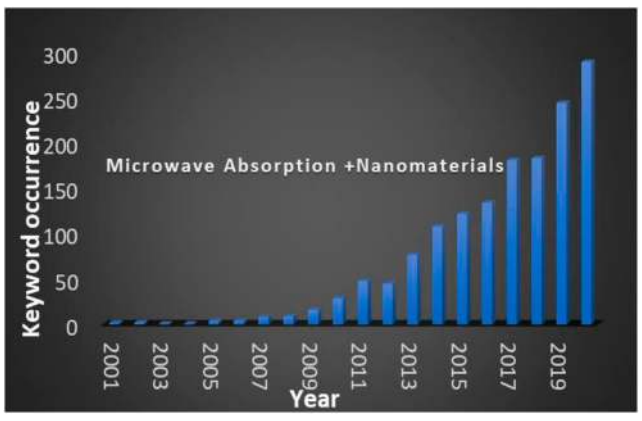


**FIGURE 1 |** Keyword occurrences from 2001 to 2020 in Scopus documents.

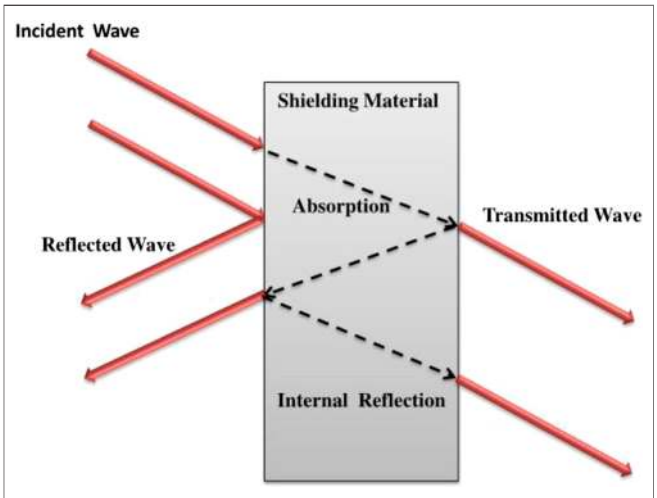


**FIGURE 2 |** Schematic illustration of electromagnetic wave propagation through a material.

reflectivity of the incident microwave (Zhao et al., 2013), achieved by the following equation:

$$\frac{\mu_1}{\varepsilon_1} = \frac{\mu_0}{\varepsilon_0}, \tag{1}$$

where $\mu_0$ and $\mu_1$ are the permeability of free space and absorber and similarly $\varepsilon_0$ and $\varepsilon_1$ are the permittivity of free space and absorbing material. In case of a perfect absorber, $\mu_1$ is equal to $\varepsilon_1$; that is, ratio of $\mu_1/\varepsilon_1$ is equal to 1. Unfortunately, at microwave frequencies, $\mu_1$ generally does not approach the magnitude of $\varepsilon_1$ (Zhao et al., 2009). Therefore, special materials and designs should be used to solve this issue. For a perfect absorber, **Eq. 1** is equal or as large as possible, but in microwave frequencies it is hard to maintain this formula because the real part ($\varepsilon_r$) of relative permittivity remains almost unchanged with the variation of microwave frequency (Zhao et al., 2009). The relationship between the permeability and permittivity of the material's impedance ($z$) (Jayalakshmi et al., 2019) is given as follows:

$$z = \sqrt{\frac{\mu_r}{\varepsilon_r}}, \tag{2}$$

$$z = z_0\sqrt{\frac{\mu_r}{\varepsilon_r}}. \tag{3}$$

Here, $\mu'$ and $\mu''$ are the real and imaginary parts of the permeability, respectively. In **Eq. 3**, $z_0$ is the impedance of free space. The relative permittivity $\varepsilon_r$, which determines how much resistance is experienced when an electrical field is generated in a vacuum, can be expressed as $\varepsilon_r = \varepsilon' - j\varepsilon''$, where $\varepsilon'$ is the actual part of permittivity and $\varepsilon''$ is the imaginary part of permittivity. Similarly, $\mu_r$ is the relative complex permeability, which measures the ability of a material to magnetize in the magnetic field, denoted as ($\mu_r = \mu' - j\mu''$). These two are important parameters to determine microwave absorption properties of an absorber. The term "relative" means the ratio of the permittivity or permeability of the material to the vacuum permittivity or permeability. $\mu'$ and $\varepsilon'$ are the capability of the material for storage of electric and magnetic field, while $\varepsilon''$ and $\mu''$ represent the loss capability of electric and magnetic fields. The root reason for the emergence of dielectric or magnetic loss is the lag of response of materials to the external field (Qin and Peng 2013). The loss tangent of the dielectric ($\delta_e$) and magnetic ($\delta_m$) material can be described as the ratio of the imaginary permittivity or permeability to the real part of permittivity and permeability, expressed as

$$\delta_e = \frac{\varepsilon''}{\varepsilon'}, \tag{4}$$

$$\delta_m = \frac{\mu''}{\mu'}. \tag{5}$$

This ratio calculates the amount of energy lost in the material to the amount stored (Zhang X.-J. et al., 2018). Conduction loss and polarization losses, such as ionic polarization, electronic polarization, and dipole orientation polarization, mainly contribute to the dielectric loss. The dissipation of electromagnetic waves is mainly affected by $\varepsilon''$ of the dielectric material. In the case of nanomaterials, more emphasis is given to the real and imaginary parts of permittivity. According to the Debye theory (Zhang X.-J. et al., 2018), $\varepsilon'$ and $\varepsilon''$ are defined as

$$\varepsilon' = \frac{\varepsilon_s - \varepsilon_\infty}{1 + (2\pi f)^2\tau^2}, \tag{6}$$

$$\varepsilon'' = \frac{2\pi f\tau(\varepsilon_s - \varepsilon_\infty)}{1 + (2\pi f)^2\tau^2}, \tag{7}$$

where $f$ is the frequency, $\varepsilon_s$ is the static permittivity, $\varepsilon_\infty$ is the dielectric constant at the infinite frequency, and $\tau$ is the polarization relaxation time. This would also aid in understanding the polarization relaxations; from this relation, dielectric material with higher conductivity, higher static dielectric constant, and medium relaxation time are beneficial for electromagnetic wave attenuation (Hu et al., 2018). By using these equations, a relationship between real and imaginary permittivity is formed:

$$\left(\varepsilon' - \frac{\varepsilon_s + \varepsilon_\infty}{2}\right)^2 + (\varepsilon'')^2 = \left(\frac{\varepsilon_s - \varepsilon_\infty}{2}\right)^2. \tag{8}$$

The plot of $\varepsilon'$ vs. $\varepsilon''$ will be a single semicircle if there is polarization relaxation, also called a Cole-Cole semicircle. A quarter wavelength (**Eq. 9**) can be used to describe the relationship between the frequency and thickness of the absorber (Zhang X. et al., 2019):

$$t_m = \frac{n\lambda}{4} = \frac{nc}{4f_m\sqrt{|\mu_r||\varepsilon_r|}}. \tag{9}$$

Here $t_m$ is the matching thickness at maximum absorption, $f_m$ is the frequency at this thickness, $\lambda$ is the wavelength of the wave, and n is an integer ($n$ = 1, 2, 3, ...). The efficiency of the absorption process results from the attenuation of electromagnetic radiation within the sample. This is directly related to the value of dielectric loss, sample thickness, and matching impedance (Hussein et al., 2020). Similarly, through proper design of the composite layer, it is possible to strongly absorb electromagnetic radiation in a spectral spectrum of interest by selecting the required thickness. For nanocomposites increasing the thickness moves the reflection loss peaks to the low frequency region (Luo et al., 2016). Also, the thickness is a parameter used to tune the absorption spectrum. Due to impedance mismatch, as a wave propagates from one medium to another medium, reflection takes place in the interface (Jayalakshmi et al., 2019). The absorption capacity can be calculated by the reflection coefficient values by means of the transmission line theory (Wu et al., 2020).

$$z_{in} = z_0\sqrt{\frac{\mu_r}{\varepsilon_r}}\tanh\left[j\frac{2\pi ft}{c}\right]\sqrt{\mu_r\varepsilon_r}, \tag{10}$$

$$\mathrm{RL}\,(dB) = 20\log\left|\frac{z_{\mathrm{in}} - z_0}{z_{\mathrm{in}} + z_0}\right|, \tag{11}$$

where $z_{\mathrm{in}}$ is the input impedance at the absorber surface, dependent on the composite electric and magnetic properties, $z_0$ is the impedance of the free space, $f'$ is the EM wave frequency,

$t$ is the thickness of the absorber, and c is the velocity of light in free space. **Equation 11** gives the reflection loss of the EM wave from the surface of a single-layer material backed with the metal conductor at the normal incidence of wave. Furthermore, attenuation factor $e^{-\alpha d}$ works on attenuating the wave amplitude with respect to traveling distance $d$, and the propagation constant, α, a key factor that represents the attenuation level (Zhou et al., 2018), another parameter used for the evaluation, can be expressed as

$$\alpha = \left(\frac{\sqrt{2}\pi f}{c}\right) \times \sqrt{\left(\mu''\varepsilon'' - \mu'\varepsilon'\right) + \sqrt{\left(\mu''\varepsilon'' - \mu'\varepsilon'\right)^2 + \left(\mu'\varepsilon'' - \mu''\varepsilon'\right)^2}}. \quad (12)$$

The test methods used to determine absorber properties can be performed by measurements of the waveguide method (Nguyen et al., 2014), free space method (Gonçalves et al., 2018), and open range RCS (Hassan et al., 2010). By using the two-port network analyzers, an experimental assessment is carried out. There are Scalar and Vector network analyzers where VNA can calculate the signal amplitude as well as the signal phase. The $S'$ parameters, dielectric permittivity, and magnetic permeability are recorded as a function of frequency (Acharya et al., 2018). $S$ parameters define an N-port network's response to a signal; for a two-port network there are four $S'$ parameters, namely, $S_{11}$, $S_{12}$, $S_{21}$, and $S_{22}$, in which the first subscript denotes the input port and the second subscript is the output port. The physical meaning of $S_{11}$ is the input reflection coefficient, $S_{12}$ is the reverse transmission from port 2 to port 1, $S_{21}$ is the forward transmission from port 1 to port 2, and $S_{22}$ is the output reflection coefficient (Caspers, 2012). The reflection coefficient (R), transmission coefficient (T), and absorption coefficient (A) can be calculated using $S$ parameters ($S_{11}$, $S_{12}$, $S_{21}$, and $S_{22}$). The coefficients are as follows (Kumar et al., 2019):

$$T = |S_{12}|^2 = |S_{21}|^2, \quad (13)$$

$$R = |S_{11}|^2 = |S_{22}|^2, \quad (14)$$

$$A = 1 - R - T. \quad (15)$$

If the multiple reflections inside the materials are neglected then

$$Ae = \frac{1 - R - T}{1 - R}. \quad (16)$$

Thus, the total shielding effect can be calculated as the sum of shielding of reflection, absorption, and multiple reflections:

$$\mathrm{SE_{total}} = \mathrm{SE}_R + \mathrm{SE}_A + \mathrm{SE}_M, \quad (17)$$

$$\mathrm{SE}_R = -10\log(1 - R), \quad (18)$$

$$\mathrm{SE}_A = -10\log(1 - Ae). \quad (19)$$

Easing the calculation of desired RAM parameters for the thorough characterization, a tool is designed (Green and Chen 2019b). They developed a python library for reflection loss characterization. libRL library takes the permittivity and permeability data from the experimentation and calculates the parameters for the full characterization of the RAM.

## HISTORICAL REVIEW (CARBON NANOTUBES)

In 1980s, limited carbon allotropic forms were available, namely, diamond, graphite, and fullerene, and the invention of fullerene expanded the number of known allotropes of carbon, in which a new cylindrical shape of carbon fullerene has been discovered, called carbon nanotubes (CNT's). The CNTs are also called nanoarchitectural allotrope of carbon with a length to diameter ratio greater than 1,000,000 (Saifuddin, Raziah, and Junizah 2012). These are generally graphite sheets, rolled up to an unbreakable hexagonal-like mesh (Donaldson et al., 2006), either open-ended or crapped. The rolling of sheets in different ways makes CNTs either metals or narrow-band semiconductors (Rahman et al., 2019). The demand for carbon nanotubes is expected to rise from USD 3.95 billion in 2017 to USD 9.84 billion by 2023, at an annual growth rate of 16.7% (CNT, n.d.), illustrating the technological role of the CNT in current era. The keyword 'carbon nanotube' appears in 160,448 documents from 1992 to 2020, as per the SCOPUS data, indicating immensity of research and applications using CNTs. Moreover, the discovery of CNT leads to a new discipline of study called "nanoscience" in the materials science field.

A paper documenting the production of multiwall carbon nanotubes (MWCNT) was published by Iijima in 1991 as key credit for the discovery of CNT. However, Radushkevish and Lukyanovich first detected and described CNTs back in 1952 (Grobert, 2007) before Iijima. Later, Lieberman studied the growth of the filaments on the carbon substrates and observed that the filament is graphite present in three different forms: tubular, twisted, and balloon-like structure (Lieberman et al., 1971) in 1971. In 1976, Oberlin et al. synthesized carbon fibers by pyrolyzing a mixture of benzene and hydrogen at ~1,100°C. The electron microscopy revealed that fibers contained different shapes and there existed a hollow tube along the fiber axis with a diameter varying from 20 to more than 500 Å (Oberlin et al., 1976). This was an important discovery in CNT research that led to the discovery of Iijima in 1991. This was the first unambiguous proof that CNTs could be developed without the need of any catalyst (Monthioux and Kuznetsov, 2006). Iijima obtained a new type of carbon structure with needle-like tubes when he was researching molecular carbon structures in the form of fullerene using the electric arc discharge technique, and the carbon atoms were arranged helically on each tube (Iijima 1991). The CNTs discovered by Iijima were called the multiwall carbon nanotubes. In 1993, after 2 years, Iijima and Ichihashi discovered the single-wall carbon nanotube (SWCNT) and announced that the synthesis of abundant single shells in the nanometer range is increasing in the gas phase. The continuation of these experiments has made major contributions to the world of science.

In general, CNTs are categorized into single-walled or multiwalled carbon nanotubes depending on the number of

tubular graphene layers. SWCNT consists of a single graphene layer with a diameter of 0.42 nm and thickness of one million times lower than diameter; and MCWNT has two or more graphene sheet layers with 3–30 nm diameter (Saifuddin et al., 2012). Structurally, MWCNT consists of many layers of graphitic carbon rolled into concentric tubes, while the SWCNT consists of a single atomic layer of graphite rolled into tubes. In general, three methods are used for the synthesis of CNT, namely, chemical vapor deposition, arc discharge (Sharma et al., 2015), and laser ablation (Scott et al., 2001). To synthesize CNTs, these methods add energy to the source carbon and combine them to form the CNT (Sharma et al., 2015).

## Carbon Nanotubes for Microwave Absorption

In this section, microwave absorption performance of CNT-based polymer nanocomposites or filler CNT matrix nanocomposites is discussed. Special features such as ability to maximize relaxation and conductivity, high aspect ratio, and high specific surface area of CNT made them reinforcement for a variety of materials, including polymers, metal/alloys, and ceramics. In determining dielectric properties, such as maximizing dielectric loss conditions (relaxation and conductivity) of the composite, morphological properties of CNT are significant (Savi et al., 2019). CNT-based polymer composites are being considered as an alternative to conventional smart materials (Ates et al., 2017). The electrical conductivity of CNTs is several orders of magnitude larger than that of all neat polymers that make up the matrix. Microwave absorption in CNTs is mostly due to dielectric loss instead of magnetic loss (Zhao et al., 2009).

Chemical vapor deposition was used to synthesize CNT/$CoFe_2O_4$ spinel nanocomposite by Che et al. (2006); high complex permittivity of $CoFe_2O_4$ helped to attain strong absorption of microwaves in the high-frequency range. The $CoFe_2O_4$/CNTs nanocomposites were homogeneously dispersed into epoxy matrix for manufacturing polymer nanocomposites and covered by a 1.4 mm thick aluminum substrate to mimic metal surface. This composite displayed a maximum loss of reflection of −18 dB at 9 GHz but offered a broad bandwidth of 7 GHz at a thickness of 1.4 mm. Sutradhar et al., in 2013, investigated the microwave properties of LZCF-CNT composite in which LZCF ($Li_{0.32}Zn_{0.26}Cu_{0.1}Fe_{2.32}O_4$) is a nanoparticle of $Cu_2^+$ doped Li–Zn ferrite. These nanoparticles were distributed into a nonmagnetic MWCNT matrix. The experimental results showed that the microwave absorption properties were strongly improved; a minimum reflection loss of −37.00 dB at 8.9 GHz and effective bandwidth of 6 GHz (RL less than −10 dB) with the sample thickness of 2 mm were observed. The improvement of the properties was attributed to a compromise between dielectric and magnetic losses. The CNTs primarily provide dielectric loss, but LZCF has magnetic loss due to the eddy current loss which is substantially greater than the dielectric loss; thus, the composites showed stronger absorption than the individual states (Sutradhar et al., 2013). Ni et al. developed and analyzed the microwave absorption and electrical and morphological characteristics of one-dimensional CNT@$BaTiO_3$ in paraffin heterostructure composite in 2015 (Ni et al., 2015). The manufacturing process is carried out by coating an acid-modified CNT with $BaTiO_3$ (CNT@$BaTiO_3$) using a sol-gel technique and the CNT@$BaTiO_3$@PANI composite nanohybrids by *in situ* aniline polymerization. They reported a minimum reflection loss of −28.90 dB at 10.7 GHz and a broad bandwidth range of 7.9 GHz–15 GHz at 3 mm sample thickness and 20 Wt.% (weight percentage). At the same time, LPA-SWCNT/$CoFe_2O_4$ nanocomposite showed better microwave properties, in which LPA is the low-pressure air arc discharge method used to synthesize the single-wall carbon nanotube, while the $CoFe_2O_4$ nanocrystals were synthesized using nitrate citric acid sol-gel autoignition method. Li et al. (2015) performed this analysis having a minimum reflection loss of −30.7 dB with a sample thickness of 2 mm lower than that of the composite CNT@$BaTiO_3$@PANI and a broad bandwidth of 7.2 GHz and used 10 Wt.% of LPA-SWCNT (S10) to achieve this result. SEM (Scanning Electron Microscopy) and TEM (Transmission Electron Microscopy) images of grown LPA-SWCNTs show several long filament-like groups, while several catalyst nanoparticles and amorphous carbon are attached to the composite in the TEM image. XRD peaks of $CoFe_2O_4$ coincided with catalysts of the 10 Wt.% LPA-SWCNTs/$CoFe_2O_4$ nanocomposites (sample S10); a weak diffraction peak is formed at about 26° corresponding to the graphite plane (0 0 2).

In 2019, Kuang et al. investigated the effect of CNT coated by extremely small FeCo-C core-shell nanoparticles and developed a simple one-step metal-organic chemical vapor deposition (MOCVD) process that will be a new way for manufacturing composites on a large scale. Considering the composite's microwave absorption properties, the minimum loss of reflection is −79.2 dB with a thickness of 2 mm for the sample (Kuang et al., 2019). The reflection value represents the absolute absorption of the incident EM waves on the sample. This was obtained with a 20 weight percentage and having a wide 6.3 GHz bandwidth. Nano-$Fe_3O_4$ compact-coated CNTs (FCCs) and $Fe_3O_4$ loose-coated CNTs (FLCs) composite for microwave absorption are investigated by Na Li et al., in 2017, prepared using a simple solvothermal method. To optimize their absorption property, FCC samples with CNT to $Fe_3$+ mass ratios ranged from 1:1 to 1:5 and were denoted as FCC11-FCC15 in which FCC14 composite provides a minimum reflection loss of -43 dB with the sample thickness of 1.5 mm. But the slight increase in thickness to 1.75 mm contributes to a broad bandwidth of 8.3 GHz from 9.7 to 18 GHz (N. Li et al., 2017), which is the highest in the CNT-based literature, **Figure 3A**. The SEM image of (FCC14) CNT to $Fe_3^+$ (1:4) is shown in **Figure 3B**, confirming that the surfaces of FCC14 are densely and tightly covered with $Fe_3O_4$ nanoparticles and no accumulation is noted. Hussein et al. researched the microwave properties of functionalized 5% MWCNT with various metal or metal alloy oxide concentrations (5%, 10%, and 20%) embedded in a polyurethane matrix in 2020. The review of the findings indicates that the absorption property has been enhanced. The reflection loss of functionalized MWCNT with 20 Wt.% of Co, Fe, and CoFe at different thicknesses is shown in **Figures 4A–C**; in each case when the concentration ranges from 5 percent to 20

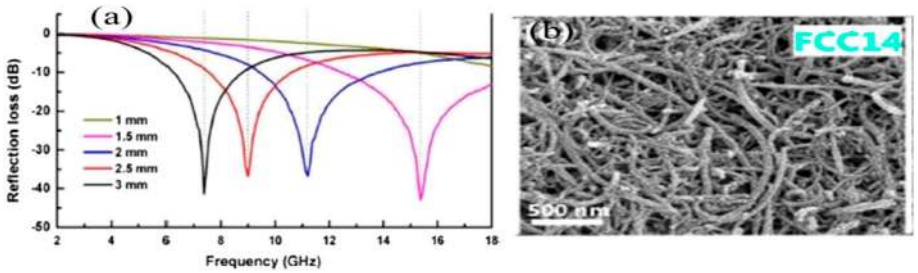


**FIGURE 3 | (A)** Reflection values of FCC14 with different thicknesses. **(B)** SEM images of (FCC14) CNT to $Fe_3$+ (1:4) (Li et al., 2017).

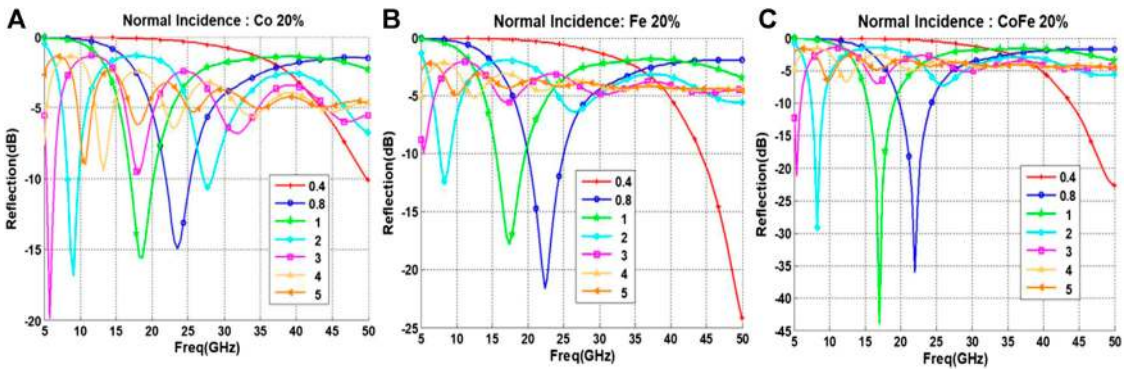


**FIGURE 4 |** Reflection loss for PU with 5% CNT with 20 wt% **(A)** Co, **(B)** Fe, and **(C)** CoFe for different thicknesses (Hussein et al., 2020).

percent, correspondingly thickness is reduced from 2 mm to 0.8 mm and also the minimum reflection value and bandwidth are improved. CoFe functionalized composite has a minimum reflection of −35 dB at 0.8 mm thickness with a bandwidth below −10 dB from 20 to 24.5 GHz. Therefore, the functionalized CNT is a promising composite for aeronautical applications (Hussein et al., 2020).

Research on CNT composites continues to use various fillers and different concentrations with different synthesis procedures to achieve a small thickness, minimum reflection coefficient, and wideband microwave absorption; it is difficult to monitor all these parameters simultaneously. Studies are accessible for the same composites but have a different outcome because of the difference in some of the parameters mentioned above, so scientists are looking for different material combinations with different parameters. The two-dimensional nanomaterials for the use of microwave absorption are discussed in the following section. **Table 1** displays more composites based on CNTs and their performances.

## 2D NANOMATERIALS

The mechanical exfoliation of graphene in 2004 exponentially increased the research interest in 2D materials (Lin et al., 2016; Choi et al., 2017; Tan et al., 2017; Hu et al., 2018). Graphene is the first 2D material isolated from graphite. There are many materials available in layered forms (Lin et al., 2016). The discovery of graphene has contributed to creating the field of 2D material. Beyond graphene, currently various 2D materials are available such as graphene-like Transition Metal Dichalcogenides, Hexagonal Boron Nitride, Graphitic Carbon Nitride, and monoelemental 2D sheets. Over the years, the number of publications related to 2D materials has increased.

The keyword "two-dimensional nanomaterial" occurrence in SCOPUS documents from 2001 to 2020 is illustrated by **Figure 5**. The electron-electron interaction in one plane leads to quantum confinement and enormous anisotropy in two dimensions due to their extensive electrical, mechanical, chemical, and physical properties (Tan et al., 2017). Increasingly, research focuses on using 2D materials in the fields of material physics, nanotechnology, and material science with applications ranging in optoelectronics, sensors, storage devices, solar cell, and so forth. Owing to their electrical behavior, large specific surface area, and low mass density (Zhang D. et al., 2019), 2D materials often have a high aspect ratio for microwave absorption applications since more atoms are bound to surface and the bound atoms have a different characteristic than others. By altering the number of atoms on the surface, specific characteristics of 2D materials can be achieved. Due to their large surface area, chemical properties can enhance interfacial polarization through the reflection and dispersion of electromagnetic waves.

**TABLE 1 |** CNT-based composites for microwave absorption.

| Nanomaterial | Performance d (mm) | Min reflection loss (dB) | Freq (GHz) | Bandwidth (GHz) | References |
|---|---|---|---|---|---|
| CNTs/$CoFe_2O_4$ | 1.4 | –18.00 | 9 | 7 | Che et al. (2006) |
| Fe filled CNT/epoxy | 1 | –31.71 | 13.2 | 2.9 | Zhao et al. (2009) |
| Defective MWCNTs/pure CI/acrylic resin | 2 | –22.20 | 14.2 | 2.4 | Li et al. (2009) |
| $Sm_2O_3$ filled MWCNTs | 3 | –14.80 | 8.2 | 2.44 | Zhang and Zhu (2009) |
| Zn–Sn substituted SrM/MWCNTs (4wt%) | 1.5 | –29.00 | 9.7 | 3 | Ghasemi (2011) |
| $Mn_{0.2}Zn_{0.8}$ $Fe_2O_4$/Ni-MWCNTs | 2 | –37.05 | 14 | 2 | Wang et al. (2012) |
| $Fe_7S_8$-$Ni_{17}S_{18}$/CNTs | 2 | –29.58 | 14.8 | 5.58 | Su et al. (2011) |
| MWCNTs)/Fe | 3.36–5.57 (4.27) | –39 | 2.68 | 2.04–3.47 (–20) (1.43) | Wen et al. (2011) |
| MWCNT/$Fe_3O_4$ hybrid | 2.0–5.0 | –41.61 | 5.5 | 3.0–11.4 (8.4) | Wang et al. (2013) |
| $Li_{0.32}Zn_{0.26}Cu_{0.1}Fe_{2.32}O_4$., LZCF-CNT | 2 | –37.00 | 8.9 | 6 | Sutradhar et al. (2013) |
| 0.25%NanocylNC7000 (MWCNT/epoxy composite) | 3 | –16.50 | 10.3 | | Che et al. (2015) |
| PANI and CNT@$BaTiO_3$/paraffin | 3 | –28.90 | 10.7 | 7.1 | Ni et al. (2015) |
| LPA-SWCNT/Co $Fe_2O_4$ | 2 | –30.7 | 13 | 7.2 | Li et al. (2015) |
| BNCNTs/$Fe_3O_4$ | 5 | –51.20 | 11.7 | | Zhang et al. (2015) |
| CdS-MWCNT (6 vol%) | 2.6 | –47.00 | | x-band | Lu et al. (2015) |
| Co/Ni @SWCNTs | 1.5 | –24.00 | | 5.6 (–20) | Singh et al. (2015) |
| MoS2/CNT nanohybrids | 2.9 | –46 | 6.6 | | Mu et al. (2017) |
| Nano-$Fe_3O_4$ compact-coated CNTs (FCC14) (30wt%) | 1.5 | –43 | | 8.3 (1.75) | Li et al. (2017) |
| $Cu_{0.25}Ni_{0.25}Zn_{0.5}$-$Fe_2O_4$/0.16% MWCNTs + epoxy | 2.5 | –37.7 | 10.20 | | Bibi et al. (2017) |
| NiCo alloy/carbon nanorod @CNT (5 Wt. % paraffin) | 2.6 | –58.80 | 14 | 6.5 | Wang L. et al. (2019) |
| $Ni_{0.5}Zn_{0.5}$ $Fe_2O_4$/MWCNT | 3 | –19.34 | 8.46 | 1.24 | Mustaffa et al. (2019) |
| CNT-small FeCo-C core-shell nanoparticles (NPs) (20wt%) | 2 | –79.2 | | 6.3 | Kuang et al. (2019) |
| Pristine CNT film and $Fe_3O_4$/CNT | 5.5 | –36.72 | 4.96 | 6.64 | Wu et al. (2020) |
| CNT/FeO/polypyrrole/carbon | 2.2 | –53.07 | 13.92 | 6.4 | Zhang et al. (2020) |
| ZnO @ MWCNTs/DA-PDMS + ZnO @ MWCNTs | 3 | –20.10 | | 8.2 to 12.4 | Zhou et al. (2020) |
| MnS2/12%CNTs | 1.4 | –63.8 | 17.4 | 4.3 | Liu et al. (2020) |
| MWCNT/$Fe_3O_4$/epoxy (2Wt.%) | | –14.4 | | 10–11 | Hekmatara et al. (2013) |
| PU+5%CNT +20% CoFe | 0.8 | –35.5 | | 4 | Hussein et al. (2020) |

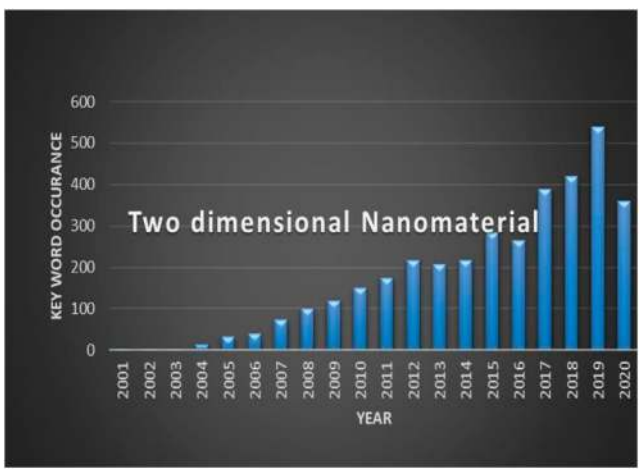


**FIGURE 5 |** Keyword occurrences in Scopus documents from 2001 to 2020.

The other advantage of 2D material is that the well-defined structure with low mass density will develop multiple reflection and dissipation of the microwaves. The third advantage is the manufacturing ability to combine 2D materials to form various composites that have multiple functionalities (Huang et al., 2019). In each year new materials are added to the list of 2D materials due to their growing research. This study deals with 2D nanomaterials, primarily graphene and MXene nanocomposites, and their microwave characteristics for absorption applications.

## Graphene

For carbon allotropes such as graphite, carbon nanotubes, and fullerenes, graphene is considered the fundamental structural unit. It is the thinnest 2D material and the discovery has undergone a revolutionary shift in the academic and industrial field. The precise history of graphene began in 1859, when Sir Benjamin Brodie discovered small graphene oxide crystals heavily covered by hydroxyl and epoxide groups. The graphite structure was discovered in 1916. Later, in 1947, Wallace explained the theory behind the existence of graphene, using the "tight binding" approximation (Randviir et al., 2014) to develop structure of electronic energy bands and Brillouin zones for graphite. In 1948, using an electron microscope, Ruess and Vogt published the world's first images of graphene. Using the micromechanical exfoliation method (Geim 2012), Fernandez-Moran extracted a millimeter-sized graphene sheet from graphite in 1960. Later more studies were conducted in this field. Boehm et al., in 1986, introduced the term graphene, deriving it from the combination of the word "graphite". Finally, in 2004, Geim and Novoselov demonstrated successful exfoliated graphene from graphite using scotch tape method, termed as a micromechanical cleavage technique (Tan et al., 2017).

They extracted a monolayer graphene sheet and for this invention, they received a Nobel Prize in 2010.

Similarly, in specific application needs, special characteristics, which cannot be provided by bare graphene, lead to the continuous research on the chemical modifications of graphene and its derivatives (Meng et al., 2018) such as graphene oxide, reduced graphene oxide, and metal-decorated graphene nanoparticle for microwave absorption applications. In the following sections, we will discuss their nanocomposites or various combinations of fillers for microwave absorption properties.

## Graphene and Graphene Derivatives Nanocomposites for Microwave Absorption

Graphene is a single-atom-thick (0.345 nm) carbon with a hexagonal structure composed of $sp^2$ hybridized carbon atoms. Each carbon atom is covalently bound with each other in the same plane (Lee et al., 2019), and it is 200 times stronger than steel. The four valence electrons in the outer shell form sigma bonds with the neighboring electrons and the fourth electron will be directly perpendicular to the sheets and delocalized (Bozzi et al., 2015). In addition to the structural uniqueness of graphene, several attractive properties are observed such as high specific theoretical surface area (2,630 $m^2 g^{-1}$), mechanical strength, high conductivity (Chen et al., 2018), high charge carrier mobility of 2000–5,000 $cm^2/V$, durability, and transparency (Bozzi et al., 2015). These properties made the graphene a suitable candidate for many applications such as sensors, energy storage, solar cell, and microwave absorption. The high electrical conductivity increases graphene's microwave absorption. Multiple reflections from the dihedral angle between nearby graphene sheets and multiple dispersions from the corrugated graphene surfaces result from the distinctive loss mechanism. Interests in graphene nanocomposites have increased recently since bare graphene as a single component does not achieve a better dispersion in the matrix, impedance mismatching due to graphene's high dielectric constant and nonmagnetic property (Bai et al., 2019). Graphene synthesis is mainly carried out by mechanical cleavage, epitaxial growth, deposition of chemical vapor, total organic synthesis, and chemical methods, discussed in detail in Zheng and Kim (2015).

Recently, there are more promising works that are developing graphene-based microwave absorbing materials. Barani et al. (2020a) reported the synthesis of epoxy-based composites using a scalable technique with a mixture of single-layer and few-layer graphene of few-micron lateral dimensions and measured the absorption efficiency in the extra high-frequency range (220–325 GHz). Composite can also work as an adhesive for the electronic components during electromagnetic interference shielding (EMI) functions. Composite achieved a total shielding efficiency of 70 dB at 320 GHz with a thickness of 1 mm and having a low graphene loading of 8 wt%. Similarly, Barani et al. (2020b) examined the multifunctional graphene at elevated temperatures using the scalable technique and the results reveal the composite at high temperature is a good candidate for packaging application of microwave components, with 19.5 vol% of filler loading composite exhibiting a total shielding efficiency of 65 dB at thickness of 1 mm in the x-band frequency range. Dual-functional graphene composite with few-layer graphene fillers is useful for the dual function applications. This composite shows a total shielding efficiency of 45 dB in the frequency range (8.2–12.4 GHz). It also provides a high thermal conductivity of 8 $Wm^{-1} k^{-1}$, so the composite can be used for both EMI shielding and heat management (Kargar et al., 2019).

Graphene oxide (GO) is considered as the product of chemical oxidation and exfoliation of layered crystalline graphite, with functional groups attached to both sides of the carbon plane and the edges (Dideikin and Vul' 2019). Functionalities such as hydroxyl, carbonyl, and carboxyl groups can increase the potential for microwave attenuation to high dipolar polarization and interfacial polarization (Hu et al., 2018). GO is also considered as an important precursor for synthesizing graphene (Du et al., 2020). Besides, the uniform integration of GO preserves its properties and overcomes the drawbacks such as shallow skin depth and extreme layer restacking. Moreover, it increases microwave absorption by dipolar polarization and the effect of Maxwell-Wanger-Sillars due to the accumulation of charge in the interfaces (Quan et al., 2018). The microwave dissipation would be impaired by serious layer restacking due to the $\pi$-$\pi$ conjugation or van der Waals interaction between the layers (Quan et al., 2018). GO has wide applications in chemistry, electricity, catalysis, and environmental pollution control and attenuation of EM waves (Cui et al., 2019). GO mainly has two significant characteristics: first, it can be produced by cheaper chemical methods using low-cost graphite as the raw material with high yields, and second, it is hydrophilic in nature. GO has been an attractive material since a simple reduction method can be used for large-scale graphene production. GO synthesis is performed by placing graphite in concentrated acid in the presence of an oxidizing agent (Habte and Ayele 2019). The preparation of GO is mainly carried out by Brodie's (Brodie 1859), Staudenmaier's (Moo et al., 2014), Hofmann's (Moo et al., 2014), Hummer's (Arthi et al., 2015; Moo et al., 2014), Modified Hummer's (Song et al., 2014), and Tour's (Habte and Ayele 2019) methods.

In recent years, research into reduced graphene oxide (rGO) has increased dramatically because it resembles pristine graphene in its mechanical and conductive characteristics. A promising material for electromagnetic wave absorption is its composites. For this application, high dielectric losses, better internal specific surface area, residual defects, and properties of oxygen-containing groups make rGO a competent material (Zhang M. et al., 2019). The harsh chemical treatments during preparation introduce severe morphological defects in the graphene sheets, leading to an increase in resistance and a decrease in conductivity with poor absorption characteristics (Ye et al., 2018). The rGO also has a high relative permittivity and impedance matching value (Zhang M. et al., 2019). By increasing the rGO loading or combining rGO with different magnetic materials, these defects can be overcome. The selection of reduction procedures that will affect the performance of rGO in material alone or a composite is important. Today, various methods of reduction, such as chemical (Tan et al., 2014), microwave (Jakhar et al., 2020), photoassisted (Xue et al., 2017), and thermal (Sengupta et al.,

2018) methods, are available. Chemical reduction is the cheapest and easily available way of reduction under normal temperatures, but due to the toxicity and explosiveness of reagents, the amount of chemical reagents used should be cautious. In particular, hydrazine and its derivatives such as hydrazine hydrate and dimethylhydrazine are used as the reagent in the chemical reduction GO (Habte and Ayele 2019). These graphene-like properties allow rGO in applications such as electronics, solar cells, batteries, biology, and EM absorbers (Tarcan et al., 2020). The recent literature on graphene and its derivatives discusses nanocomposites such as graphene-based magnetic nanocomposites (Liu P. et al., 2016; Zhang et al., 2017), graphene-based ferrite composites (Liu X. et al., 2016), graphene-based polymer composites (Chen C.-Y. et al., 2017), graphene-based ceramic composites (Feng et al., 2016), and multicomponent composites (Luo et al., 2016) and their methods of synthesis and microwave properties, as well.

Du et al. (2020) investigated the structure, morphology, and microwave properties of $Fe_3O_4$ decorated graphene. Graphene oxide is reduced to form the reduced graphene oxide and distributed over the rGO nanosheets. The nanocomposite is prepared by a one-pot hydrothermal process. Similarly, the same method was used by Fan et al. (2020) to prepare an aluminum wrapped rGO composite. The composite rGO-$Fe_3O_4$ (Du et al., 2020) reported a minimum reflection loss of −34.4 and −37.5 dB at 1.6 mm and 6.5 mm, respectively. The corresponding effective bandwidths are 3.8 GHz and 1.9 GHz. Aluminum wrapped reduced graphene oxide (Al@rGO) nanocomposite (Fan et al., 2020) has a minimum reflection loss of −46.11 dB at a frequency of 13.68 GHz with a thickness of 2 mm and an overall absorption bandwidth of 4.88 GHz at a GO (S3) content of 0.2 g. The curve below −10 dB means that 90% of the absorption of EM waves occurrs on the material. It is taken as an effective absorption bandwidth. Considering the morphology of the Al@rGO revealing a crumbled sample structure depicts the uniform distribution of Al sheet with rGO, which will enhance the surface area. The real portion of permittivity decreases by increasing frequency, but more rGO are added to increase the permittivity value, indicating the capacity to store more EM waves and impedance matching of the Al@rGO composite shows improvement over the Al alone; this contributes to the enhancement of absorption ability. Zhang et al. (2017) prepared a $CoS_2$/rGO nanohybrid using a microwave-assisted hydrothermal process, having a minimum reflection loss of the nanocomposite of −56.9 dB at 2.2 GHz, higher than Al@rGO sample, but it has a lower effective bandwidth of 4.2 GHz at 2.2 mm thickness. Composite showed a superior microwave absorption ability at a rather thin thickness.

Shu et al. (2020) investigated the microwave properties of nitrogen doped reduced graphene oxide/nickel-zinc ferrite (NRGO/$Ni_{0.5}Zn_{0.5}Fe_2O_4$) composite using the facile two-step strategy synthesis method, and this will come under the graphene-based magnetic composite. The minimum reflection coefficient value was −63.2 dB at a sample thickness of 2.91 mm with a 40% of weight percentage using paraffin matrix. The effective bandwidth is 5.4 GHz at a thickness of 2 mm; as the thickness increases the curve moves to the lower frequency and the effective bandwidth decreases. The performance of epoxy composites with hollow nanoparticles of nickel modified graphene oxide (GHN) was investigated by Zhang B. et al. (2019). The preparation is achieved effectively by incorporating the procedure of chemical etching and the process of solution blending. Polar groups of rGO sheets attract the hollow nickel particles and bind them to the rGO sheets. Further, to obtain the GHN nanocomposite, it undergoes ultrasonification.

As a good candidate for EM wave absorption applications, as shown by microwave reflection parameters, GHN has a broad bandwidth of 6.5 GHz below −10 dB at a sample thickness of 2 mm, but the minimum reflection of −33.1 dB is obtained with a higher thickness of 4.9 mm, thus decreasing the bandwidth and bringing the curve to the low frequency range. GHN10 (1:10:100) denotes the mass ratio of rGO: hollow Ni: epoxy, from the SEM image of the sample, shows that multiple interfaces are formed by the homogeneous dispersion of the GHN sample over the epoxy matrix, and it benefits from microwave absorption.

*In situ* growth method is used by Luo et al. (2016), Quan et al. (2018), and Feng et al. (2016) to prepare and examine their samples. Luo et al. developed a combination of reduced graphene oxide/strontium ferrite/polyaniline (rGO/SF/PANI) ternary nanocomposite. Quan et al. developed CoFeAl-LDH/G hybrids in which hydrotalcite-like CoFeAl-layered double hydroxide sheets (CoFeAl-LDH) are used to develop the hybrid and then an *in situ* growth on graphene oxide surfaces. Further, Wei Feng et al. investigated the rGO/ZnO composite in which rGO is covered by grain-sized *in situ* growing ZnO nanocrystals. These three samples are well distributed in the graphene derivatives studied using their TEM or SEM image samples. **Figure 6A** represents the TEM image for rGO/SF/PANI nanocomposite surface (rGO/SF nanocomposites are uniformly coated with PANI molecular chains; similarly, for CoFeAl-LDH/G, LDH sheets are uniformly dispersed into the GO surface).

To study the microwave characteristics, samples are mixed with a matrix; rGO/ZnO composite is mixed with wax of different loading mass ratio, in which 15 wt% exhibits a minimum reflection loss of −54.2 dB at a thickness of 2.4 mm with a wide band of 6.7 GHz (Feng et al., 2016). This enhancement is mainly due to the interface polarization in the rGO/ZnO interface (Feng et al., 2016). **Figure 6B** depicts rGO/SF/PANI (Luo et al., 2016) nanocomposites with 5% loading of GO and SF provides a minimum reflection loss value of −45 dB at 16 GHz with a thickness of 1.5 mm and they also have an effective bandwidth of 5.48 GHz, and the curve covers the overall Ku band. Green et al. (2020b) studied the microwave absorption of polyaniline (PANI) through a new method of Data-Driven Materials Discovery. This method is used to simulate, predict, and optimize the microwave absorption properties by mathematically modeling the EM response of the material. Using this method PANI showed a maximum reflection loss of −88.5 dB at 7.0 GHz with a thickness of 3.8 mm and a bandwidth of 2.9 GHz. By reducing the thickness to 2.1 mm the bandwidth is increased to 5.5 dB, but the maximum reflection obtained is reduced to −25.2 dB at 14.8 GHz. Similarly for poly(3,4- ethylenedioxythiophene) (Green et al.,

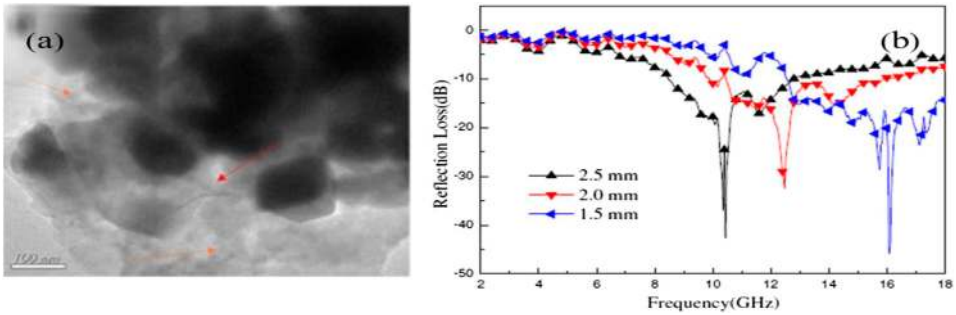


**FIGURE 6 | (A)** TEM image. **(B)** Reflection loss curve of rGO/SF/PANI composite (Luo et al., 2016).

2020c) and polypyrrole (Green et al., 2020a), Data-Driven method is applied and obtained a reflection loss of −42.6 dB and −62.6 dB at a thickness of 1.5 and 4.1, respectively. In CoFeAl-LDH/G/paraffin composite the mass ratio is varied from 40 Wt.% to 70 Wt.%, in which 50 wt.% of the sample obtained a minimum reflection loss of −23.8 dB with a thickness of 2.5 mm and had a bandwidth of 7.36 GHz. At higher frequency levels, the effective bandwidth is more prevalent.

Chen H. et al. (2017) investigated the microwave performance of a different combination of ultralight multiwall carbon nanotube and graphene foam through a facile solvothermal method. The composite forms a composite network of 1D CNT with 3D graphene foam. This network reduces the stacking of graphene sheets and strengthens the conductive path. The preparation steps include adding the solution of MWCNT ethanol to the solution of GO ethanol. In a home-made Teflon-lined autoclave, the solution is mechanically agitated for 2 h to acquire GO/MWCNT ethanol; incremental solvent exchange with water and freeze-drying was followed to obtain the final ultralight foam.

High porosity (>99%) and ultra-low bulk density (1.32–2.83 mg/cm$^3$) are seen in the prepared CGFs and the modified oxygen function group prevents agglomeration in the GO solution and disperses homogeneously. Electrical conductivity is also improved by increasing the MWCNT loading value. For a whole range of 2–18 GHz, the reflection loss is observed below −10 dB CG7F sample with a reduction temperature of 400°C, but the thickness is slightly high compared to other samples of 5 mm. At 11.6 GHz, the minimal reflection loss is −37 dB. The effect of the annealing temperature on the minimum reflection value of the CGF sample moves to higher frequency region and also decreases the productive bandwidth. The balance of thermal annealing and MWCNT content is therefore required to enhance the microwave absorption.

Additionally, the EM absorption may result in heating the electronics which, on the other hand, might lead to severe technical issues depending on the strength of EM waves, size and thermal conductivity of the absorber, and dispersion of conductive filler in the coatings. The dispersion of conductive filler such as MXenes, CNT, or graphene is pertinent to ensure that the heat flux generated due to EM absorption propagates along the filler layers toward heat sinks (Zhao et al., 2020; Balandin 2020). However, there is no report, to the best of our knowledge, investigating the effects of EM absorption and consequently heating of composites and its effects on further EM absorption. The important questions such as uniform EM absorption and subsequent uniform heating are linked to homogenous dispersion of the conductive materials. The various properties and forms of graphene and graphite derivatives nanocomposite are discussed in **Table 2**.

## MXene

The previous section addressed the capabilities of 2D graphene and graphene derivative-based nanocomposites and microwave absorption. In the recent year, a novel family of 2D material is discovered, namely, MXene, pronounced as “maxenes” (Gogotsi and Anasori 2019). It is an electrically conductive two-dimensional layered material of early transitional metal carbide/nitride or carbon nitrides. They are hydrophilic in nature due to the existence of hydroxyl or oxygen terminated surfaces (Feng et al., 2018a; Kalambate et al., 2019). The rising star among the 2D materials family was discovered by Gogotsi and his team in 2011 and they published their work “Two-Dimensional Nanocrystals Produced by Exfoliation of $Ti_3AlC_2$” (Naguib et al., 2011, 2) in the journal of Advanced Materials. These researchers made a report on 2D nanosheets having some $Ti_3C_2$ layers and conical scrolls produced the exfoliation of $Ti_3AlC_2$ in hydrofluoric acid (HF) atoms (using HF solution as an etchant and $Ti_3AlC_2$ MAX ceramic as the precursor), the etching solution done at room temperature. Al atoms are replaced by OH between the layers after HF treatment and individual $Ti_3C_2$ layers are collected, and then methanol sonification process leads to the formation of the MXene. The exfoliation phase of $Ti_3AlC_2$ (Naguib et al., 2011, 2) is the first synthesis method, which is a representative of the famous MAX phase (Feng et al., 2018b). There is no 2D material from MAX phases existing prior to this discovery.

Since 2012, the MXene-based publication has expanded enormously. The keyword appearance in SCOPUS documents from 2012 to 2020 is demonstrated in **Figure 7**. Interestingly, 450 participated in the Second International Conference on MXene, held in Beijing in May 2019, more than double the number of participants from the first conference a year before (Gogotsi and Anasori 2019). These numbers show the interest of researchers in

**TABLE 2 |** Graphene-based composites for microwave absorption.

| Nanomaterial | Performance *d* (mm) | Max RL (dB) | Freq (GHz) | Bandwidth | References |
|---|---|---|---|---|---|
| Graphene-coated Fe | 3 | –45 | 7.1 | 1.75 | Zhao et al. (2013) |
| | 2 | –27 | 11.8 | 4.4 | Zhao et al. (2013) |
| Porous graphene microflowers | 2 | –42.9 | 16 | 5.59 | Chen et al. (2017) |
| Graphitic carbon nitride (g-$C_3N_4$) nanosheets | | –36.1 | | 0.17–1.36 | Green et al. (2018c) |
| Wax and 20 wt.% $MoS_2$/graphene hybrid nanosheets | 1.6 | –55.3 | 14.5 | 2 | Zhang D. et al. (2018) |
| | 2.2 | –35 | 14.5 | 5.6 | Zhang D. et al. (2018) |
| Glass fiber/epoxy layers and graphene nanoplatelets/epoxy films | 3 | 32 | 12.2 | 8.5–16.7 (8.2) | Marra et al. (2018) |
| ERG (edge-rich graphene)/$Si_3N_4$ | 3.75 | –26.7 | | 4.2 | Ye et al. (2018) |
| $Co_2P$ nanoparticles | 1.10 | –39.3 | 15.4 | 2.4 | Green et al. (2018a) |
| Silicone rubber filled with holey graphene nanosheets (HGNS300 1 wt.%) | 3 | –45.3 | 7.8 | 3.2 | Chen et al. (2018) |
| $SrFe_{12}O_{19}$/RGO/PMMA (10 wt%) | 3.2 | 35 | | x-band | Acharya et al. (2018) |
| LDH/G-paraffin-50 | 2.5 | –23.82 | | 7.36 | Quan et al. (2018) |
| Graphene-NiS/$Ni_3S_2$ | 2.7 | –55.1 | 6 | | Zhou et al. (2018) |
| 40 wt% $WS_2$–rGO | 2.7 | –41.5 | 9.5 | | Zhang D. et al. (2019) |
| Polyaniline (PANI)/graphene aerogel (GA) | 3 | –42.3 | 11.2 | 3.2 | Wang Y.et al. (2019) |
| Plasmonic $Cu_9S_5$ nanonets/paraffin (40 wt.%) | 9.7 | –55.03 | 8.57 | 4.15 | Tao et al. (2019) |
| GHN-10/epoxy (1 wt% rGO and 10 wt% hollow nickel) | 4.9 | –33.1 | | 1.6 | Zhang B. et al. (2019) |
| | 2 | –23.8 | | 6.5 | Zhang B. et al. (2019) |
| Graphene/polyethylene glycol composite aerogels | 2.35 | –43.2 | 13.8 | 5.3 | Ji et al. (2019) |
| multilayer graphene/h-BNNP hybrid with 40 wt% of h-BNNPs | 3.29 | –67.35 | 8.04 | | Bai et al. (2019) |
| Graphene aerogel spheres with controllable hollow structures | 2.3 | –52.7 | | 7 | Li et al. (2020) |
| NRGO/$Ni_{0.5}Zn_{0.5}Fe_2O_4$/paraffine (40 wt%) | 2.91 | –63.2 | | 5.4 | Shu et al. (2020) |
| Graphene nanoplatelets in Ni/SiC composites | 1.9 | 59.15 | | 4.48 | Singh et al. (2020) |
| CoNi @NC/rGO-600 | 5.5 | –68.0 | 10.9 | 5.2 | Xu et al. (2020) |
| Al @ reduced graphene oxide | 2 | –46.11 | 13.68 | 4.88 | Fan et al. (2020) |
| rGO-$Fe_3O_4$ | 1.6 | –34.4 | | 3.8 | Du et al. (2020) |
| Hollow $Fe_3O_4$@0.125 g RGO | 2.5 | –41.89 | 6.7 | 4.2 | Cui et al. (2019) |
| $CoS_2$/rGO | 2.2 | –56.9 | | 9.1–13.2 | Zhang et al. (2017) |
| rGO/SF/PANI | 1.5 | –45 | 16.08 | 5.48 | Luo et al. (2016) |
| PANI | 2.1 | –25.2 | 14.8 | 5.5 | Green et al. (2020b) |
| | 3.8 | –88.5 | 7.0 | 2.9 | Green et al. (2020b) |
| rGO/ZnO nanocrystals/paraffin | 2.4 | –54.2 | | 6.7 | Feng et al. (2016) |
| $Co_{0.2}Ni_{0.4}Zn_{0.4}Fe_2O_4$/GN | 3.1 | –53.5 | | 4.8 GHz | Liu P. et al. (2016) |
| Poly(3,4ethylenedioxythiophene) (PEDOT) 30 wt% | 2.1 | –26.1 | 13.8 | 5.8 | Green et al. (2020c) |
| 40 wt.% | 1.5 | –42.6 | 17.0 | 3.4 | Green et al. (2020c) |
| Staudenmaier rGO | 2.5 | –37.8 | 12.3 | 4.8 | Chen et al. (2017) |
| CoNi @ dielectric Ag/graphene | 1.67 | –35 | 16 | 5.6 | Zhang N. et al. (2019) |
| Polypyrrole/paraffin (27 Wt.%) | 4.1 | –62.6 | 8.2 | 4.4 | Green et al. (2020a) |
| Polypyrrole/paraffin (30 Wt.%) | 2.6 | –56.3 | 14.2 | 6.8 | Green et al. (2020a) |
| Metal halide hybrid material $(C_6H_{13}N_4)_3Pb_2Br_7$ | 16.1 | –18.45 | | 1.0 | Lin et al. (2020) |

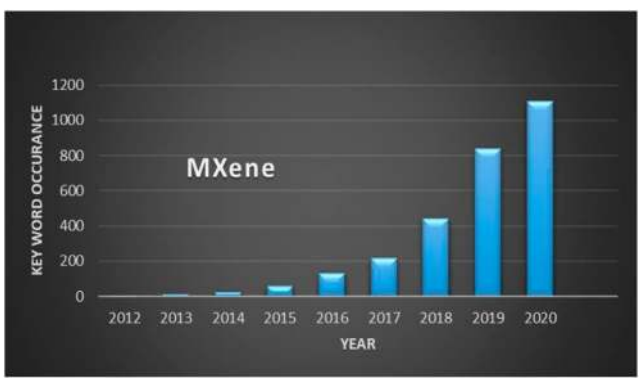


**FIGURE 7 |** Keyword occurrences for MXene in Scopus documents from 2012 to 2020.

this 2D material because of its rich chemistry, unique morphologies, good electronic conductivities (Qing et al., 2016), and similar lamellar structure with graphene (Rasid et al., 2017).

Mainly MXenes are synthesized by chemical etching of the A layers from the MAX phases (also known as nanolaminates). So far 70 members of MAX phases are experimentally produced (Qian et al., 2017), and more than 20 MXenes are synthesized. MAX phases are ternary carbides or nitrides with a general chemical formula $M_{n+1}A_n$ (Rasid et al., 2017), where n = 1, 2, or 3. M is an early transition metal (such as Ti, V, Cr, Nb, or Mo). A is an A-group element such as Al, Si, Sn, and In (generally uses the group of 13 or 14 elements) (Liu et al., 2018), and X stands for carbon and/or nitrogen. Exactly $Ti_3C_2T_x$ is the formula for MXene, where $Ti_3C_2$ is the inner structure and $T_x$ is the surface termination of OH or F groups (Feng et al., 2018b).

Max phases are closely packed multilayer structure; based on the number of M layers separated from A layers, MAX phases can be divided into $M_2AX$, $M_3AX$, and $M_4AX$, where $M_2AX$ represents 2 M layers separated from A layer and likely 3 and 4 M layers are separated for $M_3AX$ and $M_4AX$ phases; this type of MXene consisting of single transition metal are known as monotransition metal MXenes. As described above, etching is a control method in which each form of MXene differs to complete the conversion during its etching period. MXene requires solid etching with higher "n" value and needs more time for etching. Therefore, with different etching conditions, each type of MXenes demonstrates different characteristics (Xin et al., 2020).

The processing of MXenes is mainly carried out by the selective etching using different etchants. The etching method is divided into wet chemical etching, molten salt etching, and electrochemical etching (Li et al., 2019). Then a delamination process, for HF route delamination, is done by introduction of large inorganic molecules such as Dimethyl Sulfoxide (DMSO) and Tetraalkylammonium Hydroxides followed by a sonication, while for *in situ* HF route the direct use of dangerous HF etchant is to be avoided (Alhabeb et al., 2017). Since the discovery of MXenes, scientists show great interest in this material due to its widely varying properties like highly ordered structure, hydrophilicity due to the presence of termination surfaces, high metallic conductivities (~6,000–8000 S/cm) (Alhabeb et al., 2017), high stiffness, and efficient absorption of electromagnetic waves (Cui et al., 2021). These properties have made them ideal for applications such as energy storage application (Anasori et al., 2017), biomedical applications such as photothermal therapy of cancer, theragnostics, biosensors, dialysis, and neural electrodes (Huang et al., 2018), environmental applications such as photocatalysis, electrocatalysis, electronics, water purification (Zhan et al., 2020), lubrication, and water desalination, and electromagnetic wave applications such as electromagnetic interference shielding and electromagnetic wave absorption (Zhang et al., 2017).

## MXenes and Microwave Absorption

MXenes, a promising candidate application for electromagnetic wave absorption, can show dipolar and charge polarization along the thickness direction due to the different types of elements and thickness of several atomic layers (Hu et al., 2018). Moreover, the chemical reaction of $Ti_3AlC_2$ with hydrofluoric acid produces more intrinsic defects leading to strong dielectric relaxation and polarization at these areas; also the presence of termination surface enables them for tunable properties (Feng et al., 2018b); also these functional groups in multilayered structures extend interlayer spacing and lower integral density, and more tuning opportunities of microwave responses are offered (Liu et al., 2018). Bare MXene monolayers are considered to be metallic with a high electron density near the Fermi level. Thus, this suggests that the MXenes can be used as an addictive for fabricating the composites (Qing et al., 2016). So, the unique structure, defects, and metal properties made the MXene a useful option in the microwave absorption application. This section discusses MXene composites for absorption application with their structural, synthesis details.

Yang et al. (2017) used a simple tape casting method to produce a Layered Polyvinyl Butyral (PVB)/Z-type hexagonal barium ferrite $Co_2Z/Ti_3C_2$ MXene composite, where PVB acts as a composite matrix and $Co_2Z$ is hexagonal in shape and has an effective permittivity and permeability and high-frequency response that enables the use in Gigahertz range. This MXene composite is designed to use a tape casting process where $Ti_3C_2$ MXene is prepared in HF treatment by etching the Al from $Ti_3AlC_2$; then $Co_2Z$ powder is mixed uniformly in a ball mill with the solvent and dispersant.

Morphological characteristics analysis through SEM images reflects that most of the plate-like $Co_2Z$ particles are larger and have a plate-like structure in the mixture of random and plate-like $Co_2Z$ powder, while the layered $Ti_3C_2$ morphology showed that nanolayers are clearly separated from one another and the interface between phases is noticeable in the composite. Comparing PVB/$Co_2Z$, $Ti_3C_2$/PVB, and PVB/$Co_2Z$/$Ti_3C_2$ composite reflection loss values, PVB/$Co_2Z$/$Ti_3C_2$ composite has an improved absorption property with a minimum reflection loss value of −46.3 dB at 5.8 GHz with a thickness of 2.8 mm and an absorption bandwidth of 1.6 GHz. At the same time, the minimum reflection losses of $Ti_3C_2$/PVB and PVB/$Co_2Z$ are −14.4 and −32.1 dB, with thickness of 2 mm and 3 mm, respectively, and having an effective bandwidth of 0.8 and 5.6 GHz for the composites. Feng et al. (2018b) developed another $Ti_3C_2$ composite modified by Ni particles; the developed composite increased the absorption bandwidth from 5.7 GHz to 6.3 GHz with a thickness of 1.5 mm due to the synergetic dielectric and magnetic effect along with the structural effects. This modification is performed experimentally by impulsive chemical reaction between alkalized $Ti_3C_2$ MXene and Ni-ions. The characteristics of $Ti_3C_2$ nanosheet/paraffin composite are a better absorption bandwidth of 6.8 GHz with a 2 mm thickness and reflection loss of −31 dB at 12.5 GHz as shown in **Figure 8**; the improvement is due to the high dielectric loss with multiple reflection between the MXene sheets. Yan et al. (2019) fabricated a $Ti_3C_2$ composite. A single-layer $Ti_3C_2$/FCI coating was studied with different mass ratios; FCI is flaky carbonyl iron particle prepared by the high energy ball milling.

It is evident that the permittivity increases as the $Ti_3C_2$ concentration increases, resulting in a higher dielectric loss. $Ti_3C_2$ synthesis processes lead to more defects resulting in dipole polarizations in alternating field. But with the increase in the FCI component, the permeability increases. It is primarily dependent on the sample's magnetic properties. The reflection loss of the composite with a mass ratio of 1:2 indicates a minimum reflection of 15.52 at 12.8 GHz with a thickness of 1 mm and a wide band of 9.84–18.00 GHz. Similarly, $Ti_3C_2$ MXene decorated with magnetic FeCo nanoparticle was studied by He et al. (2019); their work shows an improved microwave absorption of the composite fabricated through the *in situ* hydrothermal method (He et al., 2019). The SEM image of the composite contains several nanoparticles attached to the surface of MXene, which is completely covered over the

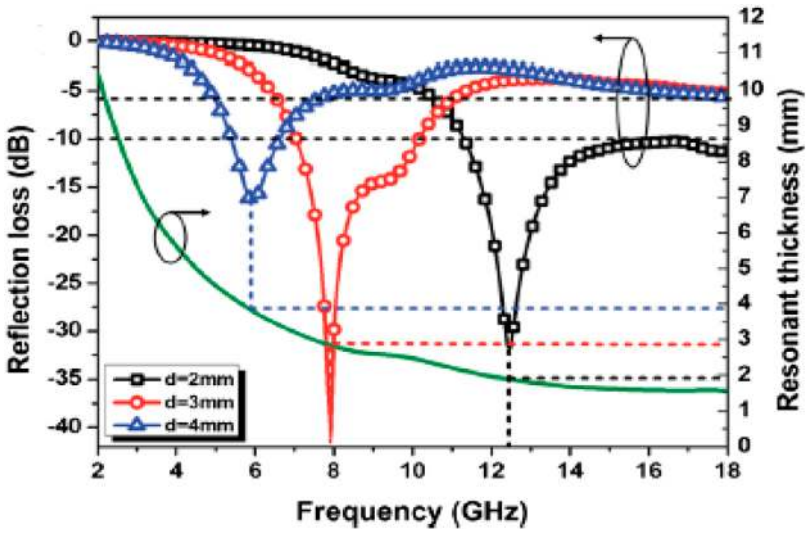


**FIGURE 8 |** Reflection loss of $Ti_3C_2$ nanosheet/paraffin composites (Feng et al., 2018a).

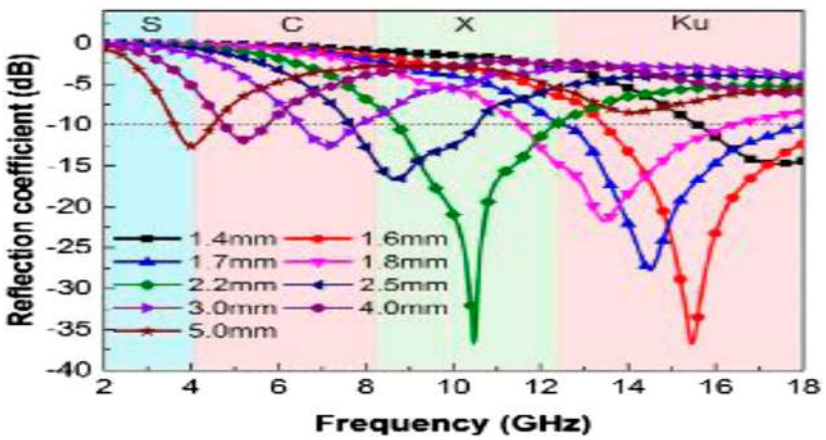


**FIGURE 9 |** Reflection coefficient of (a) 45 wt% C/$TiO_2$ hybrids (S-800) (Han et al., 2017).

MXene. Composite having a minimum reflection loss value of −17.86 dB with a thickness of 1.6 mm offers a broad absorption bandwidth of 8.8 GHz. The laminated carbon/$TiO_2$ hybrid provided by Han et al. (2017) has a loading content of 45% in the paraffin matrix; the minimum reflection coefficient reaches −36 dB at 10.5 GHz with a thickness of 2.2 mm and the effective bandwidth of 3.7 GHz. The decrease in thickness raises the bandwidth from 3.7 GHz to 5.6 GHz, but the minimum reflection changes marginally to −27.5 dB (**Figure 9**). Li et al. (2017a) prepared the same compound carbon/TiO2 with a 50% filler load, which achieved a minimum reflection of −50.3 dB with a 2.1 mm thickness, and using wax as a matrix obtained an effective bandwidth of 4.7 GHz. The $TiO_2/Ti_3C_2T_x/Fe_3O_4$ composite fabricated by Liu et al. (2018) shows minimum reflection loss of −57.3 dB at 10.1 GHz and a band width from 9.1 to 11.1 GHz at a thickness of 1.9 mm was observed. Novel hydrogenated $TiO_2$ nanocrystals are developed for microwave application (Xia et al., 2013; Xia et al., 2014). Generally, $TiO_2$ is not a good absorber but through hydrogenation, $TiO_2$ changes to an exciting MAM. This is done by a collective-movement-of-interfacial dipole (CMID) mechanism in crystalline/disordered and anatase/rutile interfaces and this introduces a collective interfacial polarization amplified microwave absorption (CIPAMA) in hydrogenated $TiO_2$. This study reveals that hydrogenated $TiO_2$ nanocrystals have higher permittivity values than the current carbonaceous MAMs. It provides a reflection loss of −37.9 dB at 13.9 GHz with a thickness of 2 mm (Tian et al., 2017). Furthermore, Al/hydrogen treated $TiO_2$ nanoparticles microwave absorption was studied. It provides a reflection loss of −58.02 dB at 6.61 GHz with a thickness of 3.1 mm (Green et al., 2019b). Similarly, $TiO_2$ nanoparticles treated with magnesium have a reflection loss of

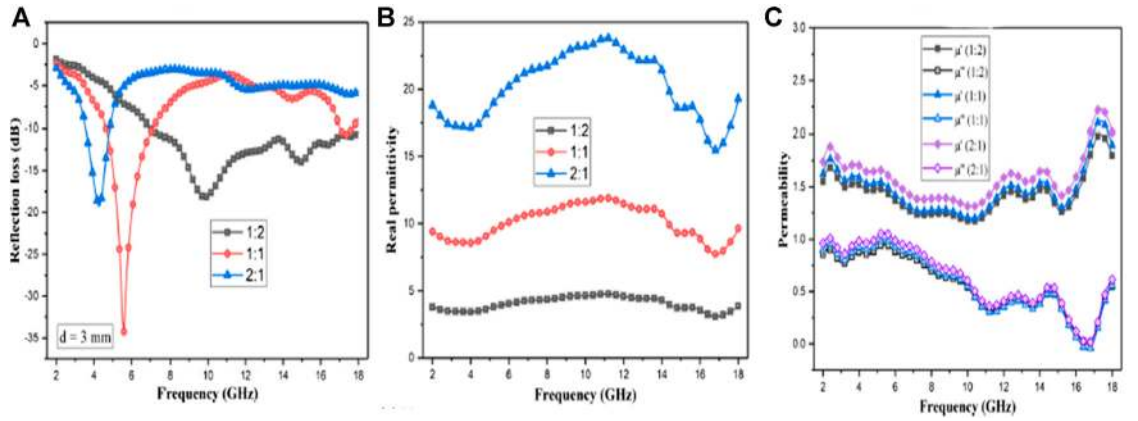


**FIGURE 10 | (A)** Reflection loss. **(B)** Real permittivity. **(C)** Real and imaginary permeability illustrations of NiO&$TiO_2$@C composites (Feng et al., 2019).

−34.69 dB at 9.07 GHz with a thickness of 1.7 mm (Green et al., 2019a).

Zhang X. et al. (2019) fabricated a $Ti_3C_2T_x$ MXene modified by *in situ* coated $Fe_3O_4$ nanoparticles and developed a simple solvothermal method for the growth of $Fe_3O_4$ nanoparticle and *in situ* heterogeneous nucleation on the $Ti_3C_2T_x$ MXene, and its performance shows a minimum reflection coefficient of −57.3 dB at 13.8 GHz with a thickness of 4.2 mm and effective bandwidth of 1.2 GHz. It is not a promising one in terms of thickness and efficient bandwidth, but it has absorption above

**TABLE 3 |** MXene-based composites for microwave absorption.

| Nanomaterial | Performance *d* (mm) | Max RL (dB) | Freq (GHz) | Bandwidth | References |
|---|---|---|---|---|---|
| $Ti_3C_2$ nanosheets filled composites | 1.4 | −11 | | 12.4–18 (5.6) | Qing et al. (2016) |
| Laminated carbon/$TiO_2$/paraffin | 2.2 | −36 | 10.5 | 8.7–12.4 (3.7) | Han et al. (2017) |
| | 1.7 | −27.5 | 14.5 | 12.4–18 (5.6) | Han et al. (2017) |
| C/$TiO_2$/wax 2.8 (w.t%) | 2.1 | −50.3 | | 4.7 | Li et al. (2017a) |
| Hydrogenated POM material (n-$Bu_4N)_2$ [$Mo_6O_{19}$] | 12.7 | −41.92 | 15.25 | | Green et al. (2020d) |
| $Ti_2$CTx/wax | 4.5 | −54.1 | | 1.1 | Li et al. (2017a) |
| $Ti_3C_2$Tx/CNTs/wax nanocomposites (35 wt%) | 1.55 | −52.9 | | 4.46 | Li et al. (2017b) |
| $Co_2$Z/PVB | 3 | −32.1 | | 5.6 | Yang et al. (2017) |
| $Ti_3C_2$/PVB | 2 | −14.4 | | 0.8 | Yang et al. (2017) |
| $Co_2$Z/$Ti_3C_2$/PVB | 2.8 | −46.3 | | 1.6 | Yang et al. (2017) |
| $Ti_3C_2$Tx MXenes/nano-carbon-spheres hybrids | 4.8 | −54.67 | 4.3 | | Dai et al. (2018) |
| Al/$H_2$ treated $TiO_2$ | 3.1 | −58.02 | 6.61 | | Green et al. (2019b) |
| Ni-modified $Ti_3C_2$ | 1.5 | −16 | | 6.3 | Feng et al. (2018b) |
| $Ti_3C_2$ MXene loaded paraffin 2.39vol% | 3 | −33 | 10.5 | 12.4–18 (5.6) | Luo et al. (2018) |
| $Ti_3C_2$ nanosheet/paraffin | 2 | −31 | 12.5 | 6.8 | Feng et al. (2018a) |
| | 3 | −40 | 7.8 | 3.2 | Feng et al. (2018a) |
| Mg/H2 treated TiO2 | 1.7 | −34.69 | 9.07 | | Green et al. (2019) |
| NiO&$TiO_2$@C paraffin | 3 | −18 | 9.9 | 11.1 | Feng et al. (2019) |
| | 2 | −25 | 15.2 | 9 | Feng et al. (2019) |
| $Ti_3C_2$Tx/polyaniline (PANI) | 1.8 | −56.3 | −13.8 | | Wei et al. (2019) |
| MXene/$Co_3O_4$/paraffin | 2 | −30 | | 10.8–17 (6.2) | Deng et al. (2019) |
| $Fe_3O_4$@$Ti_3C_2$Tx | 4.2 | −57.2 | 15.7 | 1.4 | Zhang X. et al. (2019) |
| $Ti_3C_2$ (20 wt%)/FCI (40 wt%) | 1 | −15.52 | 12.8 | 8.16 | Yan et al. (2019) |
| FeCo-$Ti_3C_2$ MXene | 1.6 | −17.86 | | 8.8 | He et al. (2019) |
| Doped, conductive $SiO_2$ | 4.2 | −55.09 | 7.5 | | Green et al. (2018d) |
| Ni nanochains/$Ti_3C_2$Tx (10%) | 1.75 | −49.9 | 11.9 | | Liang et al. (2019) |
| Ultrasmall $Fe_3O_4$ nanoparticle and MXene/$Fe_3O_4$ | 1.9 and 0.1 | −48.7 | 9.9 | | Liu P. et al. (2020) |
| PVBPS, $Ti_3C_2$Tx | 2 | −35 | | 8.2–18 (9.8) | Tan et al. (2020) |
| $Co_{0.2}Ni_{0.4}Zn_{0.4}Fe_2O_4$/ | 4.2 | −58.4 | | 2.2 | Liu et al. (2019) |
| rGO/$Nb_2CT_x$/$Fe_3O_4$ | 2.5 | −59.17 | 11.8 | 6.8 | Cui et al. (2021) |
| $TiO_2$/$Ti_3C_2T_x$/$Fe_3O_4$ | 1.9 | −57.3 | 10.1 | 9.1–11.1 | Liu et al. (2018) |
| Hydrogenated ZnO nanoparticles | 3.0 | −37.8 | 15.3 | | Xia et al. (2015) |
| Hydrogenated $TiO_2$ | 2 | −37.9 | 13.9 | | Tian et al. (2017) |
| FeP nanoparticles/paraffin wax | 2 | −37.68 | 13.6 | | Green et al. (2018b) |

90%. Li et al. (2017) synthesized a $Ti_3C_2T_x$ MXene modified by an *in situ* grown carbon nanotube composite with simple catalytic chemical vapor deposition (CVD) process. The uniform distribution of CNTs in the MXenes interlayers is seen in the processed sample. The minimum reflection loss shows a value of −52.9 dB with a thickness of 1.55 mm and an effective bandwidth of 4.46 GHz obtained with a lower filler loading of 35%. Deng et al. studied the $Ti_3C_2T_x/Co_3O_4$ composites and their microwave application performance (Deng et al., 2019). The synthesis is conducted in a concentrated strong base and argon setting through a simple and stable hydrothermal treatment. The minimum loss of reflection is −30 dB with 2 mm thickness and 10.8–17 GHz effective bandwidth, due to the multilayer structure, surface defects, conductivity of $Ti_3C_2Tx$, and capacitance of $Co_3O_4$.

A MXene-based reduced graphene oxide composite (rGO/$Nb_2CT_x/Fe_3O_4$) is prepared by Cui et al. (2021). This composite is synthesized by connecting multilayered $Nb_2CT_x$, magnetic $Fe_3O_4$ nanoparticles, and two-dimensional rGO sheets. The composite's absorption properties are attributable to the synergetic effects between the composite's multiple loss processes and the impedance matching, by covering 2D rGO on the surface increasing the impedance matching. Microwave features of the composite exhibit minimum reflection loss of −59.17 dB, indicating 99.9% absorption. It is a good candidate for microwave applications at a frequency of 11.8 GHz with a thickness of 2.5 mm and has an efficient bandwidth of 6.8 GHz.

Feng et al. (2019) prepared and studied a novel amorphous carbon-supported laminated and magnetic hybrid (represented as NiO&$TiO_2$@C). They used two-step synthesis process for producing the disordered carbon sheet using the hydrothermal oxidation at low temperature and NiO and $TiO_2$ packing in between them, using an *in situ* process, and formed the layered sandwiched structure. **Figure 10A** exhibits the reflection loss vs. frequency curve, and it shows a minimum reflection of −35 dB with a thickness of 3 mm, but the bandwidth is low with such thickness. The composite in paraffin matrix with a mass ratio of 1: 2 showed a wide effective bandwidth of 11.1 GHz and a minimum reflection loss of −18 dB at 9.9 GHz frequency. **Figure 10B** shows that the real permittivity increases by increasing the composite/paraffin mass ratio while the real permeability component follows values about 1.5, but the imaginary permeability component (**Figure 10C**) decreases at higher frequencies from 0.9 to 0.2, which will boost the matching of impedance. **Table 3** illustrates the MXene-based nanocomposites and their microwave properties.

## CONCLUSION

A comprehensive study on recent advances in the use of nanomaterials for microwave absorption has been presented, also addressing the process of microwave absorption. Microwave absorption is primarily concerned with the sample thickness, the effective bandwidth required for the desired application, and the minimum coefficient of reflection loss. Based on the applications different parametric values are needed. Thus, it is difficult to retain these parameters for a particular sample for life long, so the researchers create different combinations of composites using different fillers and filler concentrations. In the search for different materials, 2D nanomaterials with a wide range of physical, chemical, and electrical properties are discovered; in particular graphene, graphene derivatives, graphene oxide, reduced graphene oxide, and newly formed MXenes are discussed, MXene research is still in developing stage and new MXene phase members are introduced each year. For researchers, MXene is a hot subject. In order to protect the atmosphere and human life from the adverse effects of electromagnetic radiation, scientists are looking for new solutions.

## AUTHOR CONTRIBUTIONS

All three authors have contributed equally to the study and the writing of the manuscript.

## REFERENCES


Acharya, S., Ray, J., Patro, T. U., Alegaonkar, P., and Datar, S. (2018). Microwave absorption properties of reduced graphene oxide strontium hexaferrite/poly(methyl methacrylate) composites. *Nanotechnology* 29 (11), 115605. doi:10.1088/1361-6528/aaa805

Alhabeb, M., Maleski, K., Anasori, B., Lelyukh, P., Clark, L., Sin, S., et al. (2017). Guidelines for synthesis and processing of two-dimensional titanium carbide (Ti3C2Tx MXene). *Chem. Mater.* 29 (18), 7633–7644. doi:10.1021/acs.chemmater.7b02847

Anasori, B., Lukatskaya, M. R., and Gogotsi, Y. (2017). 2D metal carbides and nitrides (MXenes) for energy storage. *Nat. Rev. Mater.* 2 (2), 1–17. doi:10.1038/natrevmats.2016.98

Arthi, G., Paulchamy, B., and Lignesh, B. (2015). A simple approach to stepwise synthesis of graphene oxide nanomaterial. *J. Nanomed. Nanotech.* 6 (1), 1000253. doi:10.4172/2157-7439.1000253

Ates, M., Eker, A. A., and Eker, B. (2017). Carbon nanotube-based nanocomposites and their applications. *J. Adhes. Sci. Technol.* 31 (18), 1977–1997. doi:10.1080/01694243.2017.1295625

Bai, Y., Zhong, B., Yu, Y., Wang, M., Zhang, J., Zhang, B., et al. (2019). Mass fabrication and superior microwave absorption property of multilayer graphene/hexagonal Boron nitride nanoparticle hybrids. *Npj 2d Mater. Appl.* 3 (1), 1–10. doi:10.1038/s41699-019-0115-5

Balandin, A. A. (2020). Phononics of graphene and related materials. *ACS Nano* 14 (5), 5170–5178. doi:10.1021/acsnano.0c02718

Barani, Z., Kargar, F., Godziszewski, K., Rehman, A., Yashchyshyn, Y., Rumyantsev, S., et al. (2020a). Graphene epoxy-based composites as efficient electromagnetic absorbers in the extremely high-frequency band. *ACS Appl. Mater. Inter.* 12 (25), 28635–28644. doi:10.1021/acsami.0c06729

Barani, Z., Kargar, F., Mohammadzadeh, A., Naghibi, S., Lo, C., Rivera, B., et al. (2020b). Multifunctional graphene composites for electromagnetic shielding and thermal management at elevated temperatures. *Adv. Electron. Mater.* 6 (11), 2000520. doi:10.1002/aelm.202000520

Bibi, M., Abbas, S. M., Ahmad, N., Muhammad, B., Iqbal, Z., Rana, U. A., et al. (2017). Microwaves absorbing characteristics of metal ferrite/multiwall carbon nanotubes nanocomposites in X-band. *Composites B: Eng.* 114, 139–148. doi:10.1016/j.compositesb.2017.01.034

Bozzi, M., Pierantoni, L., and Bellucci, S. (2015). Applications of graphene at microwave frequencies. *Radioengineering* 24 (3), 661–669. doi:10.13164/re.2015.0661

Brodie, B. C. (1859). XIII. On the atomic weight of graphite. *Philos. Trans. R. Soc. Lond.* 149, 249–259. doi:10.1098/rstl.1859.0013

Caspers, F. (2012). RF engineering basic concepts: S-parameters. Available at: http://arxiv.org/abs/1201.2346

Che, B. D., Nguyen, B. Q., Nguyen, L. T., Nguyen, H. T., Nguyen, V. Q., Van Le, T., et al. (2015). The impact of different multi-walled carbon nanotubes on the X-band microwave absorption of their epoxy nanocomposites. *Chem. Cent. J.* 9 (1), 10. doi:10.1186/s13065-015-0087-2

Che, R. C., Zhi, C. Y., Liang, C. Y., and Zhou, X. G. (2006). Fabrication and microwave absorption of carbon nanotubes/CoFe2O4 spinel nanocomposite. *Appl. Phys. Lett.* 88 (3), 033105. doi:10.1063/1.2165276

Chen, C., Xi, J., Zhou, E., Peng, L., Chen, Z., and Gao, C. (2017). Porous graphene microflowers for high-performance microwave absorption. *Nanomicro Lett.* 10 (2), 26. doi:10.1007/s40820-017-0179-8

Chen, C.-Y., Pu, N.-W., Liu, Y.-M., Chen, L.-H., Wu, C.-H., Cheng, T.-Y., et al. (2018). Microwave absorption properties of holey graphene/silicone rubber composites. *Composites Part B: Eng.* 135, 119–128. doi:10.1016/j.compositesb.2017.10.001

Chen, C.-Y.Pu, N.-W., Liu, Y.-M., Huang, S.-Y., Wu, C.-H., Ger, M.-D., et al. (2017). Remarkable microwave absorption performance of graphene at a very low loading ratio. *Composites Part B: Eng.* 114, 395–403. doi:10.1016/j.compositesb.2017.02.016

Chen, H.Huang, Z., Huang, Y., Zhang, Y., Ge, Z., Qin, B., et al. (2017). Synergistically assembled MWCNT/graphene foam with highly efficient microwave absorption in both C and X bands. *Carbon* 124, 506–514. doi:10.1016/j.carbon.2017.09.007

Choi, W., Choudhary, N., Han, G. H., Park, J., Akinwande, D., and Lee, Y. H. (2017). Recent development of two-dimensional transition metal Dichalcogenides and their applications. *Mater. Today* 20 (3), 116–130. doi:10.1016/j.mattod.2016.10.002

Chojnacki, E., Huang, Q., Mukherjee, A. K., Holland, T. B., Tigner, M., and Cherian, K. (2011). Microwave absorption properties of carbon nanotubes dispersed in alumina ceramic. *Nucl. Instr. Methods Phys. Res. Section A: Acc. Spectrometers, Detectors Associated Equipment* 659 (1), 49–54. doi:10.1016/j.nima.2011.08.002

CNT (n.d.). Carbon nanotubes (CNT) market analysis | recent market developments | industry forecast to 2017-2022 | MarketsandMarketsTM. Available at: https://www.marketsandmarkets.com/Market-Reports/carbon-nanotubes-139.html (Accessed November 2, 2020).

Cui, C., Guo, R., Ren, E., Xiao, H., Zhou, M., Lai, X., et al. (2021). MXene-based RGO/Nb2CTx/Fe3O4 composite for high absorption of electromagnetic wave. *Chem. Eng. J.* 405, 126626. doi:10.1016/j.cej.2020.126626

Cui, G., Lu, Y., Zhou, W., Lv, X., Hu, J., Zhang, G., et al. (2019). Excellent microwave absorption properties derived from the synthesis of hollow Fe3o4@ Reduced graphite oxide (RGO) nanocomposites. *Nanomaterials* 9 (2), 141. doi:10.3390/nano9020141

Dai, B., Zhao, B., Xie, X., Su, T., Fan, B., Zhang, R., et al. (2018). Novel two-dimensional Ti3C2Tx MXenes/nano-carbon sphere hybrids for high-performance microwave absorption. *J. Mater. Chem. C* 6 (21), 5690–5697. doi:10.1039/C8TC01404C

Delfini, A., Albano, M., Vricella, A., Santoni, F., Rubini, G., Pastore, R., et al. (2018). Advanced radar absorbing ceramic-based materials for multifunctional applications in space environment. *Materials* 11 (9), 1730. doi:10.3390/ma11091730

Deng, R., Chen, B., Li, H., Zhang, K., Zhang, T., Yu, Y., et al. (2019). MXene/Co3O4 composite material: stable synthesis and its enhanced broadband microwave absorption. *Appl. Surf. Sci.* 488, 921–930. doi:10.1016/j.apsusc.2019.05.058

Dideikin, A. T., and Vul', A. Y. (2019). Graphene oxide and derivatives: the place in graphene family. *Front. Phys.* 6. doi:10.3389/fphy.2018.00149

Donaldson, K., Aitken, R., Tran, L., Stone, V., Duffin, R., Forrest, G., et al. (2006). Carbon nanotubes: a review of their properties in relation to pulmonary toxicology and workplace safety. *Toxicol. Sci.* 92 (1), 5–22. doi:10.1093/toxsci/kfj130

Du, Z., Chen, X., Zhang, Y., Que, X., Liu, P., Zhang, X., et al. (2020). One-pot hydrothermal preparation of Fe3O4 decorated graphene for microwave absorption. *Materials* 13 (14), 3065. doi:10.3390/ma13143065

Fan, Q., Zhang, L., Xing, H., Wang, H., and Ji, X. (2020). Microwave absorption and infrared stealth performance of reduced graphene oxide-wrapped Al flake. *J. Mater. Sci. Mater. Electron* 31 (4), 3005–3016. doi:10.1007/s10854-019-02844-2

Feng, W., Luo, H., Wang, Y., Zeng, S., Tan, Y., Deng, L., et al. (2019). Mxenes derived laminated and magnetic composites with excellent microwave absorbing performance. *Sci. Rep.* 9 (1), 3957. doi:10.1038/s41598-019-40336-9

Feng, W., Luo, H., Wang, Y., Zeng, S., Deng, L., Zhou, X., et al. (2018a). Ti3C2MXene: a promising microwave absorbing material. *RSC Adv.* 8 (5), 2398–2403. doi:10.1039/C7RA12616F

Feng, W., Luo, H., Zeng, S., Chen, C., Deng, L., Tan, Y., et al. (2018b). Ni-modified Ti3C2MXene with enhanced microwave absorbing ability. *Mater. Chem. Front.* 2 (12), 2320–2326. doi:10.1039/C8QM00436F

Feng, W., Wang, Y., Chen, J., Wang, L., Guo, L., Ouyang, J., et al. (2016). Reduced graphene oxide decorated with in-situ growing ZnO nanocrystals: facile synthesis and enhanced microwave absorption properties. *Carbon* 108, 52–60. doi:10.1016/j.carbon.2016.06.084

Geim, A. K. (2012). Graphene prehistory. *Phys. Scr.* T146, 014003. doi:10.1088/0031-8949/2012/T146/014003

Ghasemi, A. (2011). Remarkable influence of carbon nanotubes on microwave absorption characteristics of strontium ferrite/CNT nanocomposites. *J. Magnetism Magn. Mater.* 323 (23), 3133–3137. doi:10.1016/j.jmmm.2011.06.070

Gogotsi, Y., and Anasori, B. (2019). The rise of MXenes. *ACS Nano* 13 (8), 8491–8494. doi:10.1021/acsnano.9b06394

Gonçalves, F., Pinto, A., Mesquita, R. C., Silva, E., and Brancaccio, A. (2018). Free-space materials characterization by reflection and transmission measurements using frequency-by-frequency and multi-frequency algorithms. *Electronics* 7 (10), 260. doi:10.3390/electronics7100260

Green, M., and Chen, X.. (2019b). LibRL: a Python library for the characterization of microwave absorption. *J. Open Source Softw.* 4 (44): 1868. doi:10.21105/joss.01868

Green, M., and Chen, X. (2019a). Recent progress of nanomaterials for microwave absorption. *J. Materiomics* 5 (4), 503–541. doi:10.1016/j.jmat.2019.07.003

Green, M., Li, Y., Peng, Z., and Chen, X. (2020d). Dielectric, magnetic, and microwave absorption properties of polyoxometalate-based materials. *J. Magnetism Magn. Mater.* 497, 165974. doi:10.1016/j.jmmm.2019.165974

Green, M., Liu, Z., Smedley, R., Nawaz, H., Li, X., Huang, F., et al. (2018c). Graphitic carbon nitride nanosheets for microwave absorption. *Mater. Today Phys.* 5, 78–86. doi:10.1016/j.mtphys.2018.06.005

Green, M., Liu, Z., Xiang, P., Liu, Y., Zhou, M., Tan, X., et al. (2018d). Doped, conductive SiO2 nanoparticles for large microwave absorption. *Light Sci. Appl.* 7 (1), 87. doi:10.1038/s41377-018-0088-8

Green, M., Tian, L., Xiang, P., and Murowchick, J. (2018b). FeP nanoparticles: a new material for microwave absorption. *Mater. Chem. Front.* 2 (6), 1119–1125. doi:10.1039/C8QM00003D

Green, M., Tian, L., Xiang, P., Murowchick, J., Tan, X., and Chen, X. (2018a). Co2P nanoparticles for microwave absorption. *Mater. Today Nano* 1, 1–7. doi:10.1016/j.mtnano.2018.04.004

Green, M., Tran, A. T. V., and Chen, X. (2020b). Obtaining strong, broadband microwave absorption of polyaniline through data-driven materials discovery. *Adv. Mater. Inter.* 7 (18), 2000658. doi:10.1002/admi.202000658

Green, M., Tran, A. T. V., and Chen, X. (2020a). Maximizing the microwave absorption performance of polypyrrole by data-driven discovery. *Composites Sci. Technol.* 199, 108332. doi:10.1016/j.compscitech.2020.108332

Green, M., Tran, A. T. V., and Chen, X. (2020c). Realizing maximum microwave absorption of poly(3,4-ethylenedioxythiophene) with a data-driven method. *ACS Appl. Electron. Mater.* 2 (9), 2937–2944. doi:10.1021/acsaelm.0c00573

Green, M., Van Tran, A. T., Smedley, R., Roach, A., Murowchick, J., and Chen, X. (2019a). Microwave absorption of magnesium/hydrogen-treated titanium dioxide nanoparticles. *Nano Mater. Sci.* 1 (1), 48–59. doi:10.1016/j.nanoms.2019.02.001

Green, M., Xiang, P., Liu, Z., Murowchick, J., Tan, X., Huang, F., et al. (2019b). Microwave absorption of aluminum/hydrogen treated titanium dioxide nanoparticles. *J. Materiomics* 5 (1), 133–146. doi:10.1016/j.jmat.2018.12.005

Grobert, N. (2007). Carbon nanotubes - becoming clean. *Mater. Today* 10 (1), 28–35. doi:10.1016/S1369-7021(06)71789-8

Habte, A. T., and Ayele, D. W. (2019). Synthesis and characterization of reduced graphene oxide (RGO) started from graphene oxide (GO) using the Tour

method with different parameters. *Adv. Mater. Sci. Eng.*, 15. doi:10.1155/2019/5058163

Han, M., Yin, X., Li, X., Anasori, B., Zhang, L., Cheng, L., et al. (2017). Laminated and two-dimensional carbon-supported microwave absorbers derived from MXenes. *ACS Appl. Mater. Inter.* 9 (23), 20038–20045. doi:10.1021/acsami.7b04602

Han, Z., Li, D., Wang, X. W., and Zhang, Z. D.. (2011). Microwave response of FeCo/carbon nanotubes composites. *J. Appl. Phys.* 109 (7), 07A3010029. doi:10.1063/1.3533254

Hassan, N., Idris, H. A., Malek, M. F. A., Taib, M., Wan Ali, W. K., Soh, P. J., et al. (2010). Measurement of pyramidal microwave absorbers using RCS methods. *2010 Int. Conf. Intell. Adv. Syst.*, 1–5. doi:10.1109/ICIAS.2010.5716124

He, J., Shan, D., Yan, S., Luo, H., Cao, C., and Peng, Y. (2019). Magnetic FeCo nanoparticles-decorated Ti3C2 MXene with enhanced microwave absorption performance. *J. Magnetism Magn. Mater.* 492, 165639. doi:10.1016/j.jmmm.2019.165639

Hekmatara, H., Seifi, M., and Forooraghi, K. (2013). Microwave absorption property of aligned MWCNT/Fe3O4. *J. Magnetism Magn. Mater.* 346, 186–191. doi:10.1016/j.jmmm.2013.06.032

Hu, M., Zhang, N., Shan, G., Gao, J., Liu, J., Li, R. K. Y., et al. (2018). Two-dimensional materials: emerging toolkit for construction of ultrathin high-efficiency microwave shield and absorber. *Front. Phys.* 13 (4), 138113. doi:10.1007/s11467-018-0809-8

Huang, K., Li, Z., Lin, J., Han, G., and Huang, P. (2018). Two-dimensional transition metal carbides and nitrides (MXenes) for biomedical applications. *Chem. Soc. Rev.* 47 (14), 5109–5124. doi:10.1039/C7CS00838D

Huang, L., Chen, C., Li, Z., Zhang, Y., Zhang, H., Lu, J., et al. (2019). Challenges and future perspectives on microwave absorption based on two-dimensional materials and structures. *Nanotechnology* 31 (16), 162001. doi:10.1088/1361-6528/ab50af

Hussein, M. I., Jehangir, S. S., Rajmohan, I. J., Haik, Y., Abdulrehman, T., Clément, Q., et al. (2020). Microwave absorbing properties of metal functionalized-CNT-polymer composite for stealth applications. *Sci. Rep.* 10 (1), 16013. doi:10.1038/s41598-020-72928-1

Iijima, S. (1991). Helical microtubules of graphitic carbon. *Nature* 354 (6348), 56–58. doi:10.1038/354056a0

Jakhar, R., Yap, J. E., and Joshi, R. (2020). Microwave reduction of graphene oxide. *Carbon* 170, 277–293. doi:10.1016/j.carbon.2020.08.034

Jayalakshmi, C. G., Inamdar, A., Anand, A., and Kandasubramanian, B. (2019). Polymer matrix composites as broadband radar absorbing structures for stealth aircrafts. *J. Appl. Polym. Sci.* 136 (14), 47241. doi:10.1002/app.47241

Ji, H., Li, J., Zhang, J., and Yan, Y. (2019). Remarkable microwave absorption performance of ultralight graphene-polyethylene glycol composite aerogels with a very low loading ratio of graphene. *Composites A: Appl. Sci. Manufacturing* 123, 158–169. doi:10.1016/j.compositesa.2019.05.012

Kalambate, P. K., Gadhari, N. S., Li, X., Rao, Z., Navale, S. T., Shen, Y., et al. (2019). Recent advances in MXene-based electrochemical sensors and biosensors. *Trac Trends Anal. Chem.* 120, 115643. doi:10.1016/j.trac.2019.115643

Kargar, F., Barani, Z., Balinskiy, M., Magana, A. S., Lewis, J. S., and Balandin, A. A. (2019). Dual-functional graphene composites for electromagnetic shielding and thermal management. *Adv. Electron. Mater.* 5 (1), 1800558. doi:10.1002/aelm.201800558

Kuang, D., Hou, L., Wang, S., Luo, H., Deng, L., Mead, J. L., et al. (2019). Large-scale synthesis and outstanding microwave absorption properties of carbon nanotubes coated by extremely small FeCo-C core-shell nanoparticles. *Carbon* 153, 52–61. doi:10.1016/j.carbon.2019.06.105

Kumar, S., Arti, P. K., Kumar, P., Singh, N., and Verma, V. (2019). Steady microwave absorption behavior of two-dimensional metal carbide MXene and polyaniline composite in X-band. *J. Magnetism Magn. Mater.* 488, 165364. doi:10.1016/j.jmmm.2019.165364

Lee, X. J., Hiew, B. Y. Z., Lai, K. C., Lee, L. Y., Gan, S., Thangalazhy-Gopakumar, S., et al. (2019). Review on graphene and its derivatives: synthesis methods and potential industrial implementation. *J. Taiwan Inst. Chem. Eng.* 98, 163–180. doi:10.1016/j.jtice.2018.10.028

Li, G., Sheng, L., Yu, L., An, K., Ren, W., and Zhao, X. (2015). Electromagnetic and microwave absorption properties of single-walled carbon nanotubes and $CoFe_2O_4$ nanocomposites. *Mater. Sci. Eng. B* 193, 153–159. doi:10.1016/j.mseb.2014.12.008

Li, N., Huang, G.-W., Li, Y.-Q., Xiao, H.-M., Feng, Q.-P., Hu, N., et al. (2017). Enhanced microwave absorption performance of coated carbon nanotubes by optimizing the Fe3O4 nanocoating structure. *ACS Appl. Mater. Inter.* 9 (3), 2973–2983. doi:10.1021/acsami.6b13142

Li, T., Zhi, D., Chen, Y., Li, B., Zhou, Z., and Meng, F. (2020). Multiaxial electrospun generation of hollow graphene aerogel spheres for broadband high-performance microwave absorption. *Nano Res.* 13 (2), 477–484. doi:10.1007/s12274-020-2632-0

Li, X., Huang, Z., and Zhi, C. (2019). Environmental stability of MXenes as energy storage materials. *Front. Mater.* 6. doi:10.3389/fmats.2019.00312

Li, X., Yin, X., Han, M., Song, C., Sun, X., Xu, H., et al. (2017a). A controllable heterogeneous structure and electromagnetic wave absorption properties of Ti2CTxMXene. *J. Mater. Chem. C* 5 (30), 7621–7628. doi:10.1039/C7TC01991B

Li, X., Yin, X., Han, M., Song, C., Xu, H., Hou, Z., et al. (2017b). Ti3C2MXenes modified with *in situ* grown carbon nanotubes for enhanced electromagnetic wave absorption properties. *J. Mater. Chem. C* 5 (16), 4068–4074. doi:10.1039/C6TC05226F

Li, Y., Chen, C., Pan, X., Ni, Y., Zhang, S., Huang, J., et al. (2009). Multiband microwave absorption films based on defective multiwalled carbon nanotubes added carbonyl iron/acrylic resin. *Physica B: Condensed Matter* 404 (8), 1343–1346. doi:10.1016/j.physb.2008.12.015

Liang, L., Han, G., Li, Y., Zhao, B., Zhou, B., Feng, Y., et al. (2019). Promising Ti3C2Tx MXene/Ni chain hybrid with excellent electromagnetic wave absorption and shielding capacity. *ACS Appl. Mater. Inter.* 11 (28), 25399–25409. doi:10.1021/acsami.9b07294

Lieberman, M. L., Hills, C. R., and Miglionico, C. J. (1971). Growth of graphite filaments. *Carbon* 9 (5), 633–635. doi:10.1016/0008-6223(71)90085-6

Lin, H., Green, M., Xu, L. J., Chen, X., and Ma, B. (2020). Microwave absorption of organic metal halide nanotubes. *Adv. Mater. Inter.* 7 (3), 1901270. doi:10.1002/admi.201901270

Lin, Z., McCreary, A., Briggs, N., Subramanian, S., Zhang, K., Sun, Y., et al. (2016). 2D materials advances: from large scale synthesis and controlled heterostructures to improved characterization techniques, defects and applications. *2d Mater.* 3 (4), 042001, doi:10.1088/2053-1583/3/4/042001

Liu, C., Wang, B., Mu, C., Zhai, K., Wen, F., Xiang, J., et al. (2020). Enhanced microwave absorption properties of MnS2 microspheres interspersed with carbon nanotubes. *J. Magnetism Magn. Mater.* 502, 166432. doi:10.1016/j.jmmm.2020.166432

Liu, P., Yao, Z., Ng, V. M. H., Zhou, J., and Kong, L. B. (2019). Novel multilayer-like structure of Ti3C2Tx/CNZF composites for low-frequency electromagnetic absorption. *Mater. Lett.* 248, 214–217. doi:10.1016/j.matlet.2019.04.042

Liu, P., Yao, Z., Ng, V. M. H., Zhou, J., Kong, L. B., and Yue, K. (2018). Facile synthesis of ultrasmall Fe3O4 nanoparticles on MXenes for high microwave absorption performance. *Composites Part A: Appl. Sci. Manufacturing* 115, 371–382. doi:10.1016/j.compositesa.2018.10.014

Liu, J.Zhao, Z., and Zhang, L. (2020). Toward the application of electromagnetic wave absorption by two-dimension materials. *J. Mater. Sci. Mater. Electron* 27 (1). doi:10.1007/s10854-020-03800-1

Liu, P.Chen, S., Yao, M., Yao, Z., Ng, V. M. H., Zhou, J., et al. (2020). Double-layer absorbers based on hierarchical MXene composites for microwave absorption through optimal combination. *J. Mater. Res.* 35 (11), 1481–1491. doi:10.1557/jmr.2020.122

Liu, P.Yao, Z., Zhou, J., Yang, Z., and Kong, L. B. (2016). Small magnetic Co-doped NiZn ferrite/graphene nanocomposites and their dual-region microwave absorption performance. *J. Mater. Chem. C* 4 (41), 9738–9749. doi:10.1039/C6TC03518C

Liu, X.Chen, Y., Hao, C., Ye, J., Yu, R., and Huang, D. (2016). Graphene-Enhanced microwave absorption properties of Fe3O4/SiO2 nanorods. *Composites Part A: Appl. Sci. Manufacturing* 89, 40–46. doi:10.1016/j.compositesa.2016.02.006

Lu, M., Wang, X., Cao, W., Yuan, J., and Cao, M. (2015). Carbon nanotube-CdS core-shell nanowires with tunable and high-efficiency microwave absorption at elevated temperature. *Nanotechnology* 27 (6), 065702. doi:10.1088/0957-4484/27/6/065702

Luo, H., Feng, W., Liao, C., Deng, L., Liu, S., Zhang, H., et al. (2018). Peaked dielectric responses in Ti3C2 MXene nanosheets enabled composites with efficient microwave absorption. *J. Appl. Phys.* 123 (10), 104103. doi:10.1063/1.5008323

Luo, J., Shen, P., Yao, W., Jiang, C., and Xu, J. (2016). Synthesis, characterization, and microwave absorption properties of reduced graphene oxide/strontium

ferrite/polyaniline nanocomposites. *Nanoscale Res. Lett.* 11 (1), 141. doi:10.1186/s11671-016-1340-x

Marra, F., Lecini, J., Tamburrano, A., Pisu, L., and Sarto, M. S. (2018). Electromagnetic wave absorption and structural properties of wide-band Absorber made of graphene-printed glass-fibre composite. *Sci. Rep.* 8 (1), 12029. doi:10.1038/s41598-018-30498-3

Meng, F., Wang, H., Huang, F., Guo, Y., Wang, Z., Hui, D., et al. (2018). Graphene-based microwave absorbing composites: a review and prospective. *Composites Part B: Eng.* 137, 260–277. doi:10.1016/j.compositesb.2017.11.023

Monthioux, M., and Kuznetsov, V. L. (2006). Who should Be given the credit for the discovery of carbon nanotubes?. *Carbon* 44 (9), 1621–1623. doi:10.1016/j.carbon.2006.03.019

Moo, J. G., Khezri, B., Webster, R. D., and Pumera, M. (2014). Graphene oxides prepared by Hummers', Hofmann's, and Staudenmaier's methods: dramatic influences on heavy-metal-ion adsorption. *ChemPhysChem* 15 (14), 2922–2929. doi:10.1002/cphc.201402279

Mu, C., Song, J., Wang, B., Zhang, C., Xiang, J., Wen, F., et al. (2017). Two-dimensional materials and one-dimensional carbon nanotube composites for microwave absorption. *Nanotechnology* 29 (2), 025704. doi:10.1088/1361-6528/aa9a2a

Munir, A. (2017). Microwave radar absorbing properties of multiwalled carbon nanotubes polymer composites: a review. *Adv. Polym. Technol.* 36 (3), 362–370. doi:10.1002/adv.21617

Mustaffa, M. S., Azis, R. a. S., Abdullah, N. H., Ismail, I., and Ibrahim, I. R. (2019). An investigation of microstructural, magnetic and microwave absorption properties of multi-walled carbon nanotubes/Ni0.5Zn0.5Fe2O4. *Sci. Rep.* 9 (1), 15523. doi:10.1038/s41598-019-52233-2

Naguib, M., Kurtoglu, M., Presser, V., Lu, J., Niu, J., Heon, M., et al. (2011). Two-dimensional nanocrystals produced by exfoliation of Ti3 AlC2. *Adv. Mater. Weinheim* 23 (37), 4248–4253. doi:10.1002/adma.201102306

Nguyen, V. H., Hoang, M. H., Phan, H. P., Hoang, T. Q. V., and Vuong, T. P. (2014). Measurement of complex permittivity by rectangular waveguide method with simple specimen preparation. in Proceedings of the 2014 international conference on advanced technologies for communications. Hanoi, Vietnam, October 15–17, 2014. 397–400. doi:10.1109/ATC.2014.7043419

Ni, Q. Q., Zhu, Y. F., Yu, L. J., and Fu, Y. Q. (2015). One-dimensional carbon Nanotube@barium Titanate@polyaniline multiheterostructures for microwave absorbing application. *Nanoscale Res. Lett.* 10 (1), 174. doi:10.1186/s11671-015-0875-6

Oberlin, A., Endo, M., and Koyama, T. (1976). Filamentous growth of carbon through benzene decomposition. *J. Cryst. Growth* 32 (3), 335–349. doi:10.1016/0022-0248(76)90115-9

Qian, Y., Wei, H., Dong, J., Du, Y., Fang, X., Zheng, W., et al. (2017). Fabrication of urchin-like ZnO-MXene nanocomposites for high-performance electromagnetic absorption. *Ceramics Int.* 43 (14), 10757–10762. doi:10.1016/j.ceramint.2017.05.082

Qin, F., and Peng, H.-X. (2013). Ferromagnetic microwires enabled multifunctional composite materials. *Prog. Mater. Sci.* 58 (2), 183–259. doi:10.1016/j.pmatsci.2012.06.001

Qing, Y., Zhou, W., Luo, F., and Zhu, D. (2016). Titanium carbide (MXene) nanosheets as promising microwave absorbers. *Ceramics Int.* 42 (14), 16412–16416. doi:10.1016/j.ceramint.2016.07.150

Quan, B., Liang, X., Ji, G., Lv, J., Dai, S., Xu, G., et al. (2018). Laminated graphene oxide-supported high-efficiency microwave absorber fabricated by an *in situ* growth approach. *Carbon* 129, 310–320. doi:10.1016/j.carbon.2017.12.026

Rafiei-Sarmazdeh, Z., Morteza Zahedi-Dizaji, S., and Kafi Kang, A. (2019). Two-dimensional nanomaterials. *Nanostructures*. doi:10.5772/intechopen.85263

Rahman, G., Najaf, Z., Mehmood, A., Bilal, S., Shah, A., Mian, S., et al. (2019). An overview of the recent progress in the synthesis and applications of carbon nanotubes. *C–J. Carbon Res.* 5 (1), 3. doi:10.3390/c5010003

Randviir, E. P., Brownson, D. A. C., and Banks, C. E. (2014). A decade of graphene research: production, applications and outlook. *Mater. Today* 17 (9), 426–432. doi:10.1016/j.mattod.2014.06.001

Rasid, Z. A. M., Omar, M. F., Nazeri, M. F. M., A'ziz, M. A. A., and Szota, M. (2017). Low cost synthesis method of two-dimensional titanium carbide MXene. *IOP Conf. Ser. Mater. Sci. Eng.* 209, 012001. doi:10.1088/1757-899X/209/1/012001

Saifuddin, N., Raziah, A. Z., and Junizah, A. R. (2012). Carbon nanotubes: a review on structure and their interaction with proteins. *J. Chem.* 17, 1. doi:10.1155/2013/676815

Savi, P., Giorcelli, M., and Quaranta, S. (2019). Multi-walled carbon nanotubes composites for microwave absorbing applications. *Appl. Sci.* 9 (5), 851. doi:10.3390/app9050851

Scott, C. D., Arepalli, S., Nikolaev, P., and Smalley, R. E. (2001). Growth mechanisms for single-wall carbon nanotubes in a laser-ablation process. *Appl. Phys. A.* 72 (5), 573–580. doi:10.1007/s003390100761

Sengupta, I., Chakraborty, S., Talukdar, M., Pal, S. K., and Chakraborty, S. (2018). Thermal reduction of graphene oxide: how temperature influences purity. *J. Mater. Res.* 33 (23), 4113–4122. doi:10.1557/jmr.2018.338

Sharma, R., Sharma, A. K., and Sharma, V. (2015). Synthesis of carbon nanotubes by arc-discharge and chemical vapor deposition method with analysis of its morphology, dispersion and functionalization characteristics. *Cogent Eng.* 2 (1), 1094017. doi:10.1080/23311916.2015.1094017

Shu, R., Zhang, J., Guo, C., Wu, Y., Wan, Z., Shi, J., et al. (2020). Facile synthesis of nitrogen-doped reduced graphene oxide/nickel-zinc ferrite composites as high-performance microwave absorbers in the X-band. *Chem. Eng. J.* 384, 123266. doi:10.1016/j.cej.2019.123266

Silva, V. A. d., Rezende, M. C., and Cerqueira Rezende, M. (2018). Effect of the morphology and structure on the microwave absorbing properties of multiwalled carbon nanotube filled epoxy resin nanocomposites. *Mat. Res.* 21 (5), 1–9. doi:10.1590/1980-5373-mr-2017-0977

Singh, B. P., Saket, D. K., Singh, A. P., Pati, S., Gupta, T. K., Singh, V. N., et al. (2015). Microwave shielding properties of Co/Ni attached to single walled carbon nanotubes. *J. Mater. Chem. A.* 3 (25), 13203–13209. doi:10.1039/C5TA02381E

Singh, S., Maurya, A. K., Gupta, R., Kumar, A., and Singh, D. (2020). Improved microwave absorption behavioral response of Ni/SiC and Ni/SiC/graphene composites: a comparative insight. *J. Alloys Compounds* 823, 153780. doi:10.1016/j.jallcom.2020.153780

Song, J., Wang, X., and Chang, C.-T. (2014). Preparation and characterization of graphene oxide. *J. Nanomater.* 2014, 1. doi:10.1155/2014/276143

Su, Q., Li, J., Zhong, G., Du, G., and Xu, B. (2011). *In situ* synthesis of iron/nickel sulfide nanostructures-filled carbon nanotubes and their electromagnetic and microwave-absorbing properties. *J. Phys. Chem. C* 115 (5), 1838–1842. doi:10.1021/jp1113015

Sutradhar, S., Das, S., and Chakrabarti, P. K. (2013). Magnetic and enhanced microwave absorption properties of nanoparticles of Li0.32Zn0.26Cu0.1Fe2.32O4 encapsulated in carbon nanotubes. *Mater. Lett.* 95, 145–148. doi:10.1016/j.matlet.2012.12.069

Tan, C., Cao, X., Wu, X. J., He, Q., Yang, J., Zhang, X., et al. (2017). Recent advances in ultrathin two-dimensional nanomaterials. *Chem. Rev.* 117 (9), 6225–6331. doi:10.1021/acs.chemrev.6b00558

Tan, D. Q., Bora, P. J., and Daniel, Q. (2020). Enhancement of microwave absorption property of polymer blend using MXene." *Mod. Concept Mater. Sci.* 2 (4), 2020, 2020 . Available at: https://irispublishers.com/josm/fulltext/enhancement-of-microwave-absorption-property-of-polymer-blend-using-mxene.ID.000543.

Tan, S. M., Ambrosi, A., Chua, C. K., and Pumera, M. (2014). Electron transfer properties of chemically reduced graphene materials with different oxygen contents. *J. Mater. Chem. A.* 2 (27), 10668–10675. doi:10.1039/C4TA01034E

Tao, F., Green, M., Tran, A. T. V., Zhang, Y., Yin, Y., and Chen, X. (2019). Plasmonic Cu9S5 nanonets for microwave absorption. *ACS Appl. Nano Mater.* 2 (6), 3836–3847. doi:10.1021/acsanm.9b00700

Tarcan, R., Todor-Boer, O., Petrovai, I., Leordean, C., Astilean, S., and Botiz, I. (2020). Reduced graphene oxide today. *J. Mater. Chem. C* 8 (4), 1198–1224. doi:10.1039/C9TC04916A

Tian, L., Xu, J., Just, M., Green, M., Liu, L., and Chen, X. (2017). Broad range energy absorption enabled by hydrogenated TiO2 nanosheets: from optical to infrared and microwave. *J. Mater. Chem. C* 5 (19), 4645–4653. doi:10.1039/C7TC01189J

Wang, W. J., Zang, C. G., and Jiao, Q. J. (2012). Ni-coated carbon nanotubes/Mn-Zn ferrite composite as viable microwave absorbing materials. in *Advanced materials research*. Freienbach, Switzerland: Trans Tech Publications Ltd. doi:10.4028/www.scientific.net/AMR.399-401.310

Wang, Y., Du, Y., Xu, P., Qiang, R., and Han, X. (2017). Recent advances in conjugated polymer-based microwave absorbing materials. *Polymers* 9 (1), 29. doi:10.3390/polym9010029

Wang, Z., Wu, L., Zhou, J., Cai, W., Shen, B., and Jiang, Z. (2013). Magnetite nanocrystals on multiwalled carbon nanotubes as a synergistic microwave absorber. *J. Phys. Chem. C* 117 (10), 5446–5452. doi:10.1021/jp4000544

Wang, L.Wen, B., Bai, X., Liu, C., and Yang, H. (2019). NiCo alloy/carbon nanorods decorated with carbon nanotubes for microwave absorption. *ACS Appl. Nano Mater.* 2 (12), 7827–7838. doi:10.1021/acsanm.9b01842

Wang, Y.Gao, X., Fu, Y., Wu, X., Wang, Q., Zhang, W., et al. (2019). Enhanced microwave absorption performances of polyaniline/graphene aerogel by covalent bonding. *Composites Part B: Eng.* 169, 221–228. doi:10.1016/j.compositesb.2019.04.008

Wei, H., Dong, J., Fang, X., Zheng, W., Sun, Y., Qian, Y., et al. (2019). Ti3C2Tx MXene/polyaniline (PANI) sandwich intercalation structure composites constructed for microwave absorption. *Composites Sci. Technol.* 169, 52–59. doi:10.1016/j.compscitech.2018.10.016

Wen, F., Zhang, F., and Liu, Z. (2011). Investigation on microwave absorption properties for multiwalled carbon nanotubes/Fe/Co/Ni nanopowders as lightweight Absorbers. *J. Phys. Chem. C* 115 (29), 14025–14030. doi:10.1021/jp202078p

Wu, G., He, Y., Zhan, H., Shi, Q. Q., and Wang, J. N. (2020). A novel Fe3O4/carbon nanotube composite film with a cratered surface structure for effective microwave absorption. *J. Mater. Sci. Mater. Electron* 31 (14), 11508–11519. doi:10.1007/s10854-020-03698-9

Xia, T., Cao, Y., Oyler, N. A., Murowchick, J., Liu, L., and Chen, X. (2015). Strong microwave absorption of hydrogenated wide bandgap semiconductor nanoparticles. *ACS Appl. Mater. Inter.* 7 (19), 10407–10413. doi:10.1021/acsami.5b01598

Xia, T., Zhang, C., Oyler, N. A., and Chen, X. (2013). Hydrogenated TiO2 nanocrystals: a novel microwave absorbing. *Adv. Mater. Weinheim* 25 (47), 6905–6910. doi:10.1002/adma.201303088

Zhang, T.C., Oyler, N. A., and Chen, X. (2014). Enhancing microwave absorption of $TiO_2$ nanocrystals via hydrogenation. *J. Mater. Res.* 29 (18), 2198–2210. doi:10.1557/jmr.2014.227

Xin, M., Li, J., Ma, Z., Pan, L., and Shi, Y. (2020). MXenes and their applications in wearable sensors. *Front. Chem.* 8, 297. doi:10.3389/fchem.2020.00297

Xu, X., Ran, F., Fan, Z., Cheng, Z., Lv, T., Shao, L., et al. (2020). Bimetallic metal-organic framework-derived pomegranate-like nanoclusters coupled with CoNi-doped graphene for strong wideband microwave absorption. *ACS Appl. Mater. Inter.* 12 (15), 17870–17880. doi:10.1021/acsami.0c01572

Xue, B., Zou, Y., and Yang, Y. (2017). UV-assisted reduction of graphite oxide to graphene by using a photoinitiator. *J. Mater. Sci.* 52 (9), 4866–4877. doi:10.1007/s10853-016-0721-y

Yan, S., Cao, C., He, J., He, L., and Qu, Z. (2019). Investigation on the electromagnetic and broadband microwave absorption properties of Ti3C2 mxene/flaky carbonyl iron composites. *J. Mater. Sci. Mater. Electron* 30 (7), 6537–6543. doi:10.1007/s10854-019-00959-0

Yang, H., Dai, J., Liu, X., Lin, Y., Wang, J., Wang, L., et al. (2017). Layered PVB/Ba3Co2Fe24O41/Ti3C2 mxene composite: enhanced electromagnetic wave absorption properties with high impedance match in a wide frequency range. *Mater. Chem. Phys.* 200, 179–186. doi:10.1016/j.matchemphys.2017.05.057

Ye, F., Song, Q., Zhang, Z., Li, W., Zhang, S., Yin, X., et al. (2018). Direct growth of edge-rich graphene with tunable dielectric properties in porous Si3N4 ceramic for broadband high-performance microwave absorption. *Adv. Funct. Mater.* 28 (17), 1707205. doi:10.1002/adfm.201707205

Zhan, X., Si, C., Zhou, J., and Sun, Z. (2020). MXene and MXene-based composites: synthesis, properties and environment-related applications. *Nanoscale Horiz.* 5 (2), 235–258. doi:10.1039/C9NH00571D

Zhang, C., Wang, B., Xiang, J., Su, C., Mu, C., Wen, F., et al. (2017). jMicrowave absorption properties of CoS2 nanocrystals embedded into reduced graphene oxide. *ACS Appl. Mater. Inter.* 9 (34), 28868–28875. doi:10.1021/acsami.7b06982

Zhang, K., Chen, X., Gao, X., Chen, L., Ma, S., Xie, C., et al. (2020). Preparation and microwave absorption properties of carbon nanotubes/iron oxide/polypyrrole/carbon composites. *Synth. Met.* 260, 116282. doi:10.1016/j.synthmet.2019.116282

Zhang, L., and Zhu, H. (2009). Dielectric, magnetic, and microwave absorbing properties of multi-walled carbon nanotubes filled with Sm2O3 nanoparticles. *Mater. Lett.* 63 (2), 272–274. doi:10.1016/j.matlet.2008.10.015

Zhang, T., Zhong, B., Yang, J. Q., Huang, X. X., and Wen, G. (2015). Boron and nitrogen doped carbon nanotubes/Fe3O4 composite architectures with microwave absorption property. *Ceramics Int.* 41 (6), 8163–8170. doi:10.1016/j.ceramint.2015.03.031

Zhang, B.Wang, J., Wang, T., Su, X., Yang, S., Chen, W., et al. (2019). High-performance microwave absorption epoxy composites filled with hollow nickel nanoparticles modified graphene via chemical etching method. *Composites Sci. Technol.* 176, 54–63. doi:10.1016/j.compscitech.2019.04.001

Zhang, D.Jia, Y., Cheng, J., Chen, S., Chai, J., Yang, X., et al. (2018). High-performance microwave absorption materials based on MoS 2 -graphene isomorphic hetero-structures. *J. Alloys Compounds* 758, 62–71. doi:10.1016/j.jallcom.2018.05.130

Zhang, D.Liu, T., Cheng, J., Cao, Q., Zheng, G., Liang, S., et al. (2019). Lightweight and high-performance microwave absorber based on 2D WS2-RGO heterostructures. *Nano-micro Lett.* 11 (1), 38. doi:10.1007/s40820-019-0270-4

Zhang, M.Jiang, Z., Lv, X., Zhang, X., Zhang, Y., Zhang, J., et al. (2019). Microwave absorption performance of reduced graphene oxide with negative imaginary permeability. *J. Phys. D: Appl. Phys.* 53 (2), 02LT01. doi:10.1088/1361-6463/ab48a7

Zhang, N.Huang, Y., Wang, M., Liu, X., and Zong, M. (2019). Design and microwave absorption properties of thistle-like CoNi enveloped in dielectric Ag decorated graphene composites. *J. Colloid Interf. Sci.* 534, 110–121. doi:10.1016/j.jcis.2018.09.016

Zhang, X. J.Guo, A. P., Wang, G. S., and Yin, P. G. (2018). Recent progress in microwave absorption of nanomaterials: composition modulation, structural design, and their practical applications. *IET Nanodielectrics* 2 (1), 2–10. doi:10.1049/iet-nde.2018.0014

Zhang, X.Wang, H., Hu, R., Huang, C., Zhong, W., Pan, L., et al. (2019). Novel solvothermal preparation and enhanced microwave absorption properties of Ti3C2Tx MXene modified by *in situ* coated Fe3O4 nanoparticles. *Appl. Surf. Sci.* 484, 383–391. doi:10.1016/j.apsusc.2019.03.264

Zhao, B., Li, X., Zeng, S., Wang, R., Wang, L., Che, R., et al. (2020). Highly compressible polymer composite foams with thermal heating-boosted electromagnetic wave absorption abilities. *ACS Appl. Mater. Inter.* 12 (45), 50793–50802. doi:10.1021/acsami.0c13081

Zhao, D.-L., Li, X., and Shen, Z.-M. (2009). Preparation and electromagnetic and microwave absorbing properties of Fe-filled carbon nanotubes. *J. Alloys Compounds* 471 (1), 457–460. doi:10.1016/j.jallcom.2008.03.127

Zhao, X., Zhang, Z., Wang, L., Xi, K., Cao, Q., Wang, D., et al. (2013). Excellent microwave absorption property of graphene-coated Fe nanocomposites. *Sci. Rep.* 3 (1), 3421. doi:10.1038/srep03421

Zheng, Q., and Kim, J.-K. (2015). "Synthesis, structure, and properties of graphene and graphene oxide," in *Graphene for transparent conductors: synthesis, properties and Applications* (New York, NY: Springer), 29–94. doi:10.1007/978-1-4939-2769-2_2

Zhou, M., Yan, Q., Fu, Q., and Fu, H. (2020). Self-healable ZnO@ multiwalled carbon nanotubes (MWCNTs)/DA-PDMS nanocomposite via diels-alder chemistry as microwave absorber: a novel multifunctional material. *Carbon* 169, 235–247. doi:10.1016/j.carbon.2020.07.003

Zhou, S., Huang, Y., Xu, L., and Zheng, W. (2018). Microwave-assisted synthesis of graphene-NiS/Ni3S2 composites for enhanced microwave absorption behaviors through a sulfuration method. *Ceramics Int.* 44 (17), 21786–21793. doi:10.1016/j.ceramint.2018.08.281

**Conflict of Interest:** The authors declare that the research was conducted in the absence of any commercial or financial relationships that could be construed as a potential conflict of interest.